


Functional completeness of planar Rydberg blockade structures

Simon Stastny¹, Hans Peter Büchler¹, and Nicolai Lang^{1*}

*Institute for Theoretical Physics III and Center for Integrated Quantum Science and Technology,
University of Stuttgart, 70550 Stuttgart, Germany*

 (Received 5 January 2023; revised 4 August 2023; accepted 4 August 2023; published 25 August 2023)

The construction of Hilbert spaces that are characterized by local constraints as the low-energy sectors of microscopic models is an important step towards the realization of a wide range of quantum phases with long-range entanglement and emergent gauge fields. Here we show that planar structures of trapped atoms in the Rydberg blockade regime are functionally complete: Their ground-state manifold can realize any Hilbert space that can be characterized by local constraints in the product basis. We introduce a versatile framework, together with a set of provably minimal logic primitives as building blocks, to implement these constraints. As examples, we present lattice realizations of the string-net Hilbert spaces that underlie the surface code and the Fibonacci anyon model. We discuss possible optimizations of planar Rydberg structures to increase their geometrical robustness.

DOI: [10.1103/PhysRevB.108.085138](https://doi.org/10.1103/PhysRevB.108.085138)

I. INTRODUCTION

Recent advances in the control of single atoms and their coherent manipulation [1–5] are the technological foundation for applications such as quantum simulation [6–9], high-precision metrology [10,11], and, hopefully, future quantum computers [12–15]. For any of these applications, suitable platforms must offer fine-grained control over their degrees of freedom, dynamically tunable interactions, and the possibility to decouple the environment. Promising in this regard are arrays of individually trapped, neutral atoms that can be manipulated by optical tweezers [1,3] and excited into Rydberg states [16,17]. These exhibit strong interactions, which lead to the Rydberg blockade mechanism where excited atoms prevent their neighbors within a tunable radius from being excited [18–22]. In this paper, we study on very general grounds the theoretical capabilities of the Rydberg platform in the blockade regime and demonstrate its versatility by constructing the gauge-invariant Hilbert spaces of two models with Abelian and non-Abelian topological order.

Encouraged by the fast development and scalability of the Rydberg platform (see e.g., Refs. [23–25]), there has been increased interest in identifying promising near-term applications for the NISQ era [26]. Among the many applications of two-dimensional arrays of Rydberg atoms, the field of *geometric programming* and the design of *synthetic quantum matter* have been identified as promising candidates to leverage the capabilities of available and upcoming NISQ platforms.

The rationale of geometric programming is the solution of algorithmic problems by encoding them into the geometry of the atomic array. This direction of research is founded on the insight that due to the Rydberg blockade, the ground states

of these systems naturally map to *maximum independent sets* (MIS) on so called *unit disk graphs* [27]; finding MIS is a long-known optimization problem in graph theory that has been shown to be NP-hard [28]. This makes the computation of ground-state energies of Rydberg arrangements NP-hard as well [29], but also opens the possibility to tackle a variety of other hard optimization problems [30–35] by polynomial-time reductions to the MIS problem [36]. First solutions of MIS instances on various graphs in two and three dimensions have been demonstrated in experiments recently [37–39], and a quantitative comparison of experimental solutions with classical algorithms suggest a superlinear quantum speedup for some classes of graphs [39].

A very different application of the Rydberg blockade mechanism is the engineering of synthetic quantum matter on the single-atom level [40]. The potential of this approach has been demonstrated recently by Verresen *et al.* [41] (related results were reported by Samajdar *et al.* [42]), who proposed the realization of topological spin liquids on delicately designed lattice structures of atoms. In this scenario, the Rydberg blockade enforces a dimer constraint (the local gauge constraint of an odd \mathbb{Z}_2 lattice gauge theory [43]), which, in combination with quantum fluctuations, can give rise to long-range entangled many-body states with Abelian topological order. First experimental results were reported shortly after [44], accompanied by theoretical studies of the used quadiabatic preparation schemes [45,46].

This paper is written from and motivated by the synthetic quantum matter perspective, but its results apply to geometric programming as well. Our starting point is the question whether other local constraints (besides the dimer constraint) can be realized on the Rydberg platform. To find an answer, we first formalize the problem and then use this formulation to derive our main result, namely that *every* local constraint that can be encoded by a Boolean function can be implemented in the ground-state manifold of a planar arrangement

*nicolai.lang@itp3.uni-stuttgart.de

of atoms in the blockade regime. Crucial for this result is the existence of a structure that implements the truth table of a NOR-gate (“Not OR”) in its ground-state manifold. While our proof is constructive, it does typically not yield optimal (= small) solutions. We therefore expand on our main result and compile a comprehensive list of provably minimal structures that realize all important primitives of Boolean logic. Together with a structure that facilitates the crossing of two “wires” within the plane, these primitives provide a toolbox to build structures that satisfy more complicated constraints. As an example, we construct a system with a ground-state manifold that is locally isomorphic to the gauge-invariant Hilbert space of an even \mathbb{Z}_2 lattice gauge theory, i.e., the charge-free sector of the toric code [47]. With a similar construction, we tailor a pattern of atoms with a ground-state manifold isomorphic to the string-net Hilbert space of the “golden string-net model [48]”; a system that, with added quantum fluctuations, could support non-Abelian Fibonacci anyons. Having constructed all these structures, we briefly discuss possibilities to numerically optimize their geometries to make them more robust against geometric imperfections and the effects of long-range van der Waals interactions.

II. RATIONALE AND OUTLINE

Here we illustrate the rationale of the paper and provide a brief outline of its main results without technical overhead. Readers interested in the details can skip forward to Sec. III. Readers only interested in specific applications can read this section first and then skip to Sec. VII or Sec. IX.

In this paper, we consider two-dimensional arrangements of trapped atoms that can either be in their electronic ground state or excited into a Rydberg state (*Rydberg structures*). We focus on systems without quantum fluctuations, where the ground states are determined by local detunings and Rydberg blockade interactions (Sec. III). The detunings lower the energy for atoms in the Rydberg state by an atom-specific amount, and the Rydberg blockade interaction forbids atoms closer than a specific distance to be excited simultaneously. The interplay of these two contributions singles out ground states that are characterized by excitations patterns where no additional atom can be excited without violating the Rydberg blockade, and where the sum of the detunings of the excited atoms is maximal (so called *maximum-weight independent sets*). There can be different configurations that minimize the energy, hence the ground-state manifold is typically degenerate. In this paper, we ask which ground-state manifolds such structures can realize and, conversely, how to tailor structures that realize a prescribed ground-state manifold (Sec. IV).

A simple example is given in Fig. 1(a) where the position of the atoms is shown in (i); the two atoms are constrained by the Rydberg blockade (gray circles) and cannot be excited simultaneously (indicated by the black edge connecting them). The color of the atoms encodes their detuning; here both atoms lower the energy of the system by Δ when excited into the Rydberg state (blue nodes). In (ii) we show the two excitation patterns that minimize the energy (orange nodes denote excited atoms). Note that the atoms cannot be excited simultaneously due to the Rydberg blockade. If one lists the ground-state configurations in a table, where each

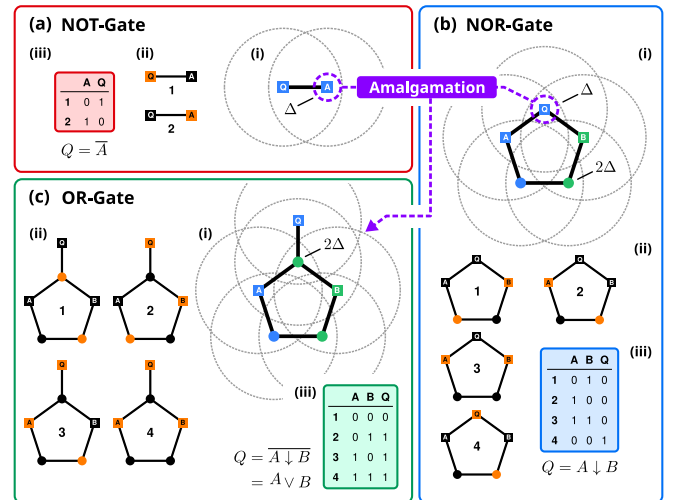


FIG. 1. Rationale. (a) Structure of two atoms (i) with local detunings Δ (blue vertices) that are in Rydberg blockade (gray circles); the blockade is indicated by a black edge connecting the atoms. The ground-state manifold (ii) is given by patterns of excited atoms (orange) that minimize the energy; here it is twofold degenerate. The two ground-state configurations realize the truth table (iii) of a NOT-gate $Q = \bar{A}$. (b) Structure of five atoms (i) with local detunings Δ (blue) and 2Δ (green) in a ring-like Rydberg blockade. The ground-state manifold (ii) is fourfold degenerate. If one selects the three labeled atoms and identifies them with the columns of the table in (iii), the four ground-state configurations realize the truth table of a NOR-gate $Q = A \downarrow B = \overline{A \vee B}$. (c) Joining the output atom of the NOR-gate with the input atom of the NOT-gate (and adding their detunings) yields a new structure that realizes the truth table of an OR-gate: $Q = \overline{A \downarrow B} = A \vee B$. This construction is called *amalgamation*.

column corresponds to an atom and each row to a ground-state configuration, we find the “truth table” of a Boolean NOT-gate $Q = \bar{A}$. Here we interpret one of the atoms as “input” (A) and the other as “output” (Q).

This concept generalizes to more complicated Boolean gates [Fig. 1(b)]: Consider the five atoms in a ring-like blockade (i). Three of the atoms (blue) lower the energy by Δ , two (green) by 2Δ when excited. By inspection one finds the four degenerate ground-state configurations in (ii). This is promising as truth tables of Boolean gates that operate on two bits have four rows. However, they only have three columns (two for the inputs of the gate and one for its output). We therefore select three of the five atoms by assigning labels to them: A and B play the role of the inputs and Q is the output. We call atomic structures with designated input/output atoms *Rydberg complexes* [49] (Sec. V A). If we list the four ground-state configurations of these three atoms, we find the truth table of a NOR-gate $Q = A \downarrow B = \overline{A \vee B}$ in (iii). Note that the remaining two atoms (we call them *ancillas*)—while not contributing independent degrees of freedom—are still necessary to realize this specific ground-state manifold. At this point things get interesting because it is a well-known fact of Boolean algebra that the NOR-gate is *functionally complete* (just like the NAND-gate): Every Boolean function can be decomposed into a circuit build from NOR-gates only.

To leverage this decomposition, we need a method to combine “gate complexes” to form larger “circuit complexes”;

we call this procedure *amalgamation* (Sec. VB). A simple example is shown in Fig. 1(c) where we attach the NOT-gate from Fig. 1(a) to the output of the NOR-gate in Fig. 1(b) (note that the detunings of the atoms that are joined add up). Using the detunings and blockades in (i) yields the four degenerate ground-state configurations in (ii). When we label the inputs of the NOR-gate again by A and B, and now focus on the output Q of the attached NOT-gate, we find indeed the truth table of an OR-gate $Q = A \downarrow B = A \vee B$ in (iii). Thus we can parallel the logical composition of gates by a geometrical combination of atomic structures such that the relation between ground-state configurations and truth tables remains intact. In combination with the insight that every Boolean circuit can be drawn in the plane without crossing lines (after suitable augmentations), this allows us to show that the truth table of any Boolean function can be realized as the ground-state manifold of a suitably designed atomic structure. This *functional completeness* is our first main result and motivates the title of the paper (Sec. VI).

For instance, the *existence* of a structure that realizes the truth table of an OR-gate is a corollary of functional completeness. However, the *specific* construction as the combination of a NOR-gate and a NOT-gate in Fig. 1(c) raises the questions whether this particular realization with six atoms is *unique* and whether it is *minimal* (in the sense that the same truth table could not be realized with fewer atoms). The answer to the first question is negative: There are geometrically different structures that realize the same truth table in their ground-state manifold. The answer to the second question is positive, though: We show that it is impossible to implement this truth table with less than six atoms. Note that the functional completeness implies the existences of structures for *all* common gates of Boolean logic (such as AND, XOR, etc.). We take this as motivation to construct provably minimal structures for all these primitives (Secs. VII and VIII). Together with the procedure of amalgamation, these equip our versatile toolbox to engineer more complicated structures.

Our second important contribution is an application of the functional completeness as a tool to engineer synthetic quantum matter (Sec. IX). Many interesting quantum phases in two dimension are characterized by hidden patterns of long-range entanglement, known as topological order. These patterns can give rise to anyonic excitations, which make such systems potential substrates for quantum memories and even quantum computers. A large class of entanglement patterns can be understood as condensates of extended objects (like strings). A crucial first step for the realization of these phases is therefore the preparation of Hilbert spaces spanned by states of such extended objects. However, in experiments, we typically start from Hilbert spaces with a local tensor product structure (for example, an array of two-level atoms). Our only hope is to make the extended objects emerge due to interactions in the low-energy sector of a suitably designed physical system. This often boils down to enforce local *gauge symmetries*, which single out states that can be interpreted in terms of extended objects. Such local constraints can be reformulated as Boolean functions that must be satisfied by the states of the local degrees of freedom of the underlying system. For any constraint of this form, our functional completeness result ensures the existence of a structure of atoms, interacting via the Rydberg blockade mechanism, that realizes this constraint

in its ground-state space. It is then just a matter of copying and joining these structures in a translational invariant way to tessellate the plane. The ground-state manifolds of such tessellations can therefore implement a large class of nontrivial Hilbert spaces on which condensation (driven by quantum fluctuations) might lead to topologically ordered many-body quantum phases. Using our toolbox developed in the first part of the paper, we demonstrate this construction explicitly for the Abelian toric code phase (Sec. IX A) and the non-Abelian, computationally universal Fibonacci anyon model (Sec. IX B).

The truth tables realized by the ground states of all atomic structures presented in this paper depend on the positions of the atoms. (Because these positions define which pairs are in blockade and which atoms can be excited simultaneously.) However, the *exact* placement is often ambiguous. For example, consider the structure in Fig. 1(ai), which realizes the NOT-gate. It is clear that the blockade constraint (black edge) does not change if the atoms are slightly shifted, as long as the blockade radii (gray circles) encompass both atoms. We refer to the set of atom positions as the *geometry* of a structure and argue that “robust” geometries should avoid distances between atoms that are close to the critical blockade distance. For the complexes in Fig. 1, this translates into the geometric objective to maximize the distances between nodes and gray circles. We formalize this notion by assigning a number to geometries that quantifies their “robustness” (Sec. X A) and numerically construct optimized geometries that maximize this number (Sec. X B).

We conclude the paper with an outline of open questions, directions for further research (Sec. XI), and a brief summary (Sec. XII).

III. PHYSICAL SETTING

We consider planar arrangements of trapped atoms with repulsive van der Waals interactions when excited into the Rydberg state [2,50]. Every atom is assigned an index $i \in V = \{1 \dots N\}$, placed at position $\mathbf{r}_i \in \mathbb{R}^2$, and described by a two-level system $|n\rangle_i$ where $n = 0$ corresponds to the electronic ground state and $n = 1$ the excited Rydberg state.

The quantum dynamics of such systems is achieved by coupling the electronic ground state to the Rydberg state by external laser fields with Rabi frequency Ω_i and detuning Δ_i for each atom [51–53]. Here we are mainly interested in the regime $\Omega_i \rightarrow 0$ where the Hamiltonian reduces to

$$H[C] = - \sum_i \Delta_i n_i + \sum_{i < j} U(|\mathbf{r}_i - \mathbf{r}_j|) n_i n_j. \quad (1)$$

Note that we assume the detunings Δ_i to be site dependent [54,55]. This Hamiltonian acts on the full Hilbert space $\mathcal{H} = (\mathbb{C}^2)^{\otimes N}$ with the representation $n_i = |1\rangle\langle 1|_i$. The configuration of the system is completely specified by $\mathcal{C} \equiv (\mathbf{r}_i, \Delta_i)_{i \in V}$ to which we refer as (*Rydberg*) *structure*; the position data $G_{\mathcal{C}} \equiv (\mathbf{r}_i)_{i \in V}$ alone is the *geometry* of the structure \mathcal{C} (Fig. 2). For atoms in the Rydberg state, the interaction potential in Eq. (1) is $U_{\text{vdW}}(r) = C_6 r^{-6}$ with $C_6 > 0$ the coupling strength of the van der Waals interaction; we refer to $H[C]$ with $U = U_{\text{vdW}}$ as the *van der Waals (vdW) model*. However, in many situations a simplified model $U = U_{\infty}$ with

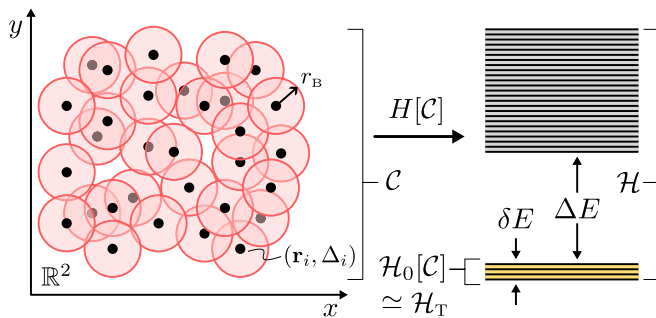


FIG. 2. Setting and objective. A two-dimensional structure $\mathcal{C} = (\mathbf{r}_i, \Delta_i)_{i \in V}$ of atoms $i \in V$ with position \mathbf{r}_i and detuning Δ_i is governed by the Hamiltonian $H[\mathcal{C}]$ that describes the Rydberg blockade interaction with blockade radius r_B . The Hamiltonian gives rise to a low-energy eigenspace $\mathcal{H}_0[\mathcal{C}] \subset \mathcal{H}$ of width δE , separated from the excited states by a gap ΔE . The objective of this paper is the construction of a structure \mathcal{C} from a given target Hilbert space \mathcal{H}_T such that $\mathcal{H}_0[\mathcal{C}] \simeq \mathcal{H}_T$.

$U_\infty(r \geq r_B) = 0$ and $U_\infty(r < r_B) = \infty$ with *blockade radius* r_B is a reasonable approximation for the low-energy physics of Eq. (1); we refer to $H[\mathcal{C}]$ with $U = U_\infty$ as the *PXP model* [41,56]. In this paper, we use the PXP model unless stated otherwise. We discuss valid choices for the blockade radius r_B in Sec. X A where we optimize the geometry of structures to limit the effects of residual van der Waals interactions.

In the PXP model, the effect of the van der Waals interactions is approximated by a kinematic constraint that is completely encoded by a *blockade graph* $B = (V, E)$, where an edge $e = (i, j) \in E$ between atoms $i, j \in V$ indicates that they are in blockade, i.e., their distance is smaller than the blockade radius r_B . An abstract graph that can be realized in this way is called a *unit disk graph* (not every graph has this property); conversely, a geometry G_C that realizes a prescribed graph as its blockade graph is a *unit disk embedding* of this graph (the “unit” here is the blockade radius r_B). Throughout the paper, the blockade graph of a structure will be drawn by black edges connecting atoms that are in blockade.

IV. DEFINITION OF THE PROBLEM

The primary goal of this paper is to find structures \mathcal{C} such that there is a well-separated low-energy eigenspace $\mathcal{H}_0[\mathcal{C}]$ of $H[\mathcal{C}]$ where $\mathcal{H}_0[\mathcal{C}]$ satisfies certain prescribed properties that we describe in detail below. We quantify the separation of $\mathcal{H}_0[\mathcal{C}]$ by its spectral width δE and its gap ΔE to the rest of the spectrum (Fig. 2). Note that the experimental prerequisites for the construction of arbitrary structures \mathcal{C} are already in place [4,54,55,57]. If one would switch on a weak drive $\delta E < \Omega_i \ll \Delta E$, this would induce quantum fluctuations between the states of the Hilbert space $\mathcal{H}_0[\mathcal{C}]$, potentially giving rise to many-body states with interesting properties. In this paper, we do not study such quantum effects but focus on the implementation of the subspace $\mathcal{H}_0[\mathcal{C}]$. We specify the eigenspace to construct in terms of a *target Hilbert space* \mathcal{H}_T ,

$$\mathcal{H}_0[\mathcal{C}] \stackrel{!}{\simeq} \mathcal{H}_T. \quad (2)$$

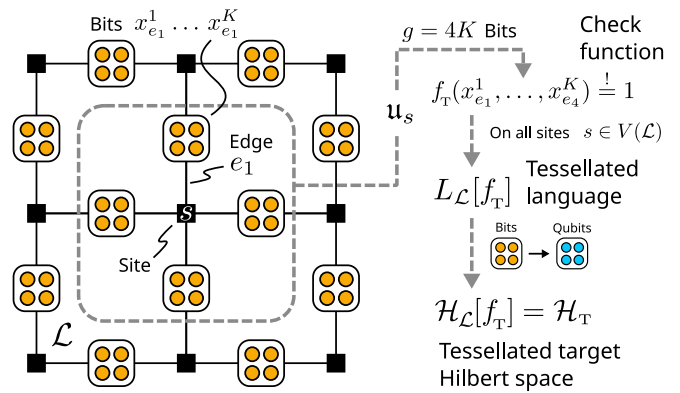


FIG. 3. Tessellated language and target Hilbert space. A tessellated target Hilbert space \mathcal{H}_T is a subspace of the full Hilbert space of K qubits placed on each edge of a square lattice \mathcal{L} ; it is spanned by product states $|\mathbf{x}\rangle$ of bit patterns $\mathbf{x} \in L_{\mathcal{C}}[f_T]$. The tessellated language $L_{\mathcal{C}}[f_T]$ comprises all bit patterns $\mathbf{x} \in \mathbb{F}_2^g$ that locally satisfy the Boolean check function $f_T : \mathbb{F}_2^g \rightarrow \mathbb{F}_2$. The $g = 4K$ arguments of the check function on each site s are singled out by the bit-projector \mathbf{u}_s .

Informally speaking, our goal is to “solve” this equation for structures \mathcal{C} for given \mathcal{H}_T . To make this possible, the target Hilbert space \mathcal{H}_T must be specifiable in a form that we define in the remainder of this section.

Formal languages. Throughout the paper we make use of the notion of (formal) languages [58] on the binary alphabet $\mathbb{F}_2 = \{0, 1\}$. A *word* $\mathbf{x} \equiv (x_1 x_2 \dots x_n) \equiv x_1 x_2 \dots x_n \in \mathbb{F}_2^n$ is a finite string of *letters* $x_i \in \mathbb{F}_2$ (the set of all such finite strings is denoted \mathbb{F}_2^*). A (*formal*) *language* L is then simply a collection of words: $L \subseteq \mathbb{F}_2^*$. Here we only consider *uniform* languages with words that have all the same length. For example, $L_{\text{CPY}} := \{000, 111\} \subset \mathbb{F}_2^3$ is a uniform language of words with length $n = 3$, $\mathbf{x} = (111)$ is a word in L_{CPY} and $x_1 = 1$ is the first letter of \mathbf{x} . The words $\mathbf{y} = (011) \in \mathbb{F}_2^3$ and $\mathbf{z} = (0000) \in \mathbb{F}_2^4$ are not in this language: $\mathbf{y}, \mathbf{z} \notin L_{\text{CPY}}$. The subscript “CPY” stands for “copy” and hints at the role this language will play later.

Other examples are the class of languages generated by the truth tables of Boolean functions. Let $w : \mathbb{F}_2^{n-1} \rightarrow \mathbb{F}_2$ be an arbitrary Boolean function of $n - 1$ variables; then

$$L[w] := \{x_1 \dots x_{n-1} y \mid y = w(x_1, \dots, x_{n-1})\} \subset \mathbb{F}_2^n \quad (3)$$

is the language generated from the rows of the truth table of w , where the first $n - 1$ letters of each word correspond to the input \mathbf{x} and the last letter encodes the output $w(\mathbf{x})$. A language of this class always has 2^{n-1} words of uniform length n . Note that the “copy” language L_{CPY} is *not* of the form Eq. (3).

Another special class is given by *tessellated languages* on lattices. In the following, we introduce the concept exemplarily for a finite square lattice \mathcal{L} with periodic boundaries; the generalization to other lattices and boundary conditions is straightforward. Start by associating K classical bits to every edge $e \in E(\mathcal{L})$ of the lattice (Fig. 3). A bit configuration of the system $\mathbf{x} \in \mathbb{X}_{\mathcal{L}} = \mathbb{F}_2^{K|E(\mathcal{L})} \subset \mathbb{F}_2^*$ assigns every bit a Boolean value x_e^i ($i = 1 \dots K$). We focus on the family of uniform languages $L \subseteq \mathbb{X}_{\mathcal{L}}$ that can be characterized by a Boolean function that is local in the following sense: For a site $s \in V(\mathcal{L})$ of the square lattice, let the *bit-projector*

$u_s(\mathbf{x}) = (x_{e_1}^1, \dots, x_{e_4}^K)$ single out the (ordered) set of $g = 4K$ bits on the four edges e_i emanating from s . Let $f : \mathbb{F}_2^g \rightarrow \mathbb{F}_2$ be an arbitrary Boolean function of g arguments, henceforth referred to as *check function*. The tessellated language of bit patterns on \mathcal{L} generated by f is then defined as

$$L_{\mathcal{L}}[f] := \{\mathbf{x} \in \mathbb{X}_{\mathcal{L}} \mid \forall s \in V(\mathcal{L}) : f(u_s(\mathbf{x})) = 1\}. \quad (4)$$

In words: $L_{\mathcal{L}}[f]$ is the set of bit patterns on the lattice \mathcal{L} that locally satisfy the constraints imposed by f .

Target Hilbert spaces. To any uniform language $L \subseteq \mathbb{F}_2^n$ we can naturally associate the linear subspace of states on n qubits (or spin- $1/2$)

$$\mathcal{H}(L) := \text{span}\{|\mathbf{x}\rangle \mid \mathbf{x} \in L\} \subseteq (\mathbb{C}^2)^{\otimes n}. \quad (5)$$

For example, $\mathcal{H}(L_{\text{CPY}}) = \text{span}\{|000\rangle, |111\rangle\}$ is the two-dimensional subspace on three qubits spanned by product states with configurations in $L_{\text{CPY}} = \{000, 111\}$. By contrast, the Hilbert space $\mathcal{H}' = \text{span}\{(|000\rangle + |111\rangle)/\sqrt{2}\}$ is not of the form (5).

We require the target Hilbert space \mathcal{H}_T , that we aim to realize as ground-state manifold $\mathcal{H}_0[\mathcal{C}]$, to be specified by a language L_T according to Eq. (5),

$$\mathcal{H}_T = \mathcal{H}(L_T). \quad (6)$$

We are particularly interested in the special class of *tessellated* target Hilbert spaces given in terms of tessellated languages that are generated by a check function (Fig. 3),

$$\mathcal{H}_T = \mathcal{H}_{\mathcal{L}}[f_T] := \mathcal{H}(L_{\mathcal{L}}[f_T]). \quad (7)$$

Recall that these languages come equipped with a spatial structure (in the sense that the *bits* are located on the edges of a lattice \mathcal{L}). This spatial structure is inherited by the Hilbert space $\mathcal{H}_{\mathcal{L}}[f_T]$ viewed as state space of a system where K qubits are placed on every edge of \mathcal{L} .

For example, the Hilbert space $\mathcal{H}_{\mathbb{Z}_2}$ of the even \mathbb{Z}_2 lattice gauge theory is a particular subspace of a Hilbert space that describes a system of qubits on the edges of a square lattice (i.e., $K = 1$ and $g = 4$). $\mathcal{H}_{\mathbb{Z}_2}$ is spanned by the product states of patterns of qubits in the state $|1\rangle$ that form closed loops [59]. $\mathcal{H}_{\mathbb{Z}_2}$ is an admissible tessellated target Hilbert space because we can realize $\mathcal{H}_{\mathbb{Z}_2} = \mathcal{H}_{\mathcal{L}}[f_{\mathbb{Z}_2}]$ with the check function

$$f_{\mathbb{Z}_2}(x_1, x_2, x_3, x_4) = 1 \oplus x_1 \oplus x_2 \oplus x_3 \oplus x_4, \quad (8)$$

where \oplus denotes modulo-2 addition (Exclusive-OR or XOR); the bit-projector $u_s(\mathbf{x})$ simply singles out the four bits on edges emanating from site s ,

$$u_s \left(\begin{array}{c} \text{---} \overset{x_{e_1}^1}{\bullet} \text{---} \\ \text{---} \overset{x_{e_2}^1}{\bullet} \text{---} \\ \text{---} \overset{x_{e_3}^1}{\bullet} \text{---} \\ \text{---} \overset{x_{e_4}^1}{\bullet} \text{---} \end{array} \right) = (x_{e_1}^1, x_{e_2}^1, x_{e_3}^1, x_{e_4}^1). \quad (9)$$

Physically, Eq. (8) enforces Gauss's law on a charge-free background by forbidding strings of qubits in state $|1\rangle$ to end on a site. Further examples for tessellated target Hilbert spaces are the more general "string-net" Hilbert spaces that can describe a large variety of topological orders and deconfined gauge theories [48].

V. RYDBERG COMPLEXES

Before we can tackle our main goal, namely the construction of tessellated Rydberg structures \mathcal{C} with $\mathcal{H}_0[\mathcal{C}] \simeq \mathcal{H}_T = \mathcal{H}_{\mathcal{L}}[f_T]$ for a given check function f_T , we first need to specify the notion of a finite Rydberg *complex* as a preliminary step. Specific examples for Rydberg complexes can be found throughout the remainder of the paper.

A. From structures to complexes

Consider the language $L_{\text{CPY}} = \{000, 111\}$ and let $\mathcal{H}_{\text{CPY}} = \mathcal{H}(L_{\text{CPY}}) = \text{span}\{|000\rangle, |111\rangle\}$ be our target Hilbert space. Our goal is to realize \mathcal{H}_{CPY} as the ground-state manifold $\mathcal{H}_0[\mathcal{C}_{\text{CPY}}]$ of a structure \mathcal{C}_{CPY} of $n = 3$ atoms. This, however, is impossible: Since $|111\rangle \in \mathcal{H}_{\text{CPY}}$, none of the three atoms can be in blockade with each other. Consequently, $\mathcal{H}_0[\mathcal{C}_{\text{CPY}}]$ cannot contain only the states $|000\rangle$ and $|111\rangle$ (Appendix A 1). This problem is not specific to the language L_{CPY} but shared by many (although not all) languages. The solution is to consider *larger* structures of $N \geq n$ atoms and to identify the letters of words with a *subset* of n distinguished atoms (we call them *ports*); the remaining $N - n$ atoms play then the role of *ancillas*. A structure together with a distinguished set of ports will be referred to as a (*Rydberg*) *complex*.

Let us formalize this notion. Consider a structure \mathcal{C} of N atoms and a language $L \subseteq \mathbb{F}_2^n$ of words of uniform length $n \leq N$. Let $\mathcal{L} = \{A, B, \dots\}$ denote a set of n labels where each label is associated with a fixed letter position of words in L . (If one prints all words of L as rows of a table, the labels correspond to the column headers.) Let $\ell : \mathcal{L} \rightarrow V$ be an injective label function that assigns a label to a subset of n atoms (the *ports*); the $N - n$ atoms without labels are the *ancillas*. We refer to the structure \mathcal{C} together with the labeling ℓ as a (*Rydberg*) L -*complex* \mathcal{C}_L if the states that span $\mathcal{H}_0[\mathcal{C}]$ can be identified by the configurations of the ports alone,

$$\mathcal{H}_0[\mathcal{C}_L] \equiv \mathcal{H}_0[\mathcal{C}] = \text{span}\{|\mathbf{x}, a(\mathbf{x})\rangle \in \mathcal{H} \mid \mathbf{x} \in L\}. \quad (10)$$

In $|\mathbf{x}, a(\mathbf{x})\rangle$, the state of ports is given by the first n bits \mathbf{x} (in some fixed order) and the state of ancillas by a $N - n$ bit-valued function $a : L \rightarrow \mathbb{F}_2^{N-n}$. The ground-state space $\mathcal{H}_0[\mathcal{C}_L]$ will be referred to as an L *manifold*. An important aspect of this definition is that the ancillas do *not* introduce additional low-energy degrees of freedom; they are only needed to unleash the full potential of the blockade interactions. In this sense, we say that a complex $\mathcal{C}_T \equiv \mathcal{C}_{L_T}$ *realizes* a target Hilbert space $\mathcal{H}_T = \mathcal{H}(L_T)$ and write

$$(\mathbb{C}^2)^{\otimes N} \supseteq \mathcal{H}_0[\mathcal{C}_T] \simeq \mathcal{H}_T = \mathcal{H}(L_T) \subseteq (\mathbb{C}^2)^{\otimes n} \quad (11)$$

with the isomorphism \simeq given by $|\mathbf{x}, a(\mathbf{x})\rangle \leftrightarrow |\mathbf{x}\rangle$. If we say that a complex realizes a *language* L , we mean that it realizes the target Hilbert space $\mathcal{H}_T = \mathcal{H}(L)$ defined by this language.

As an example, consider again the "copy" language $L_{\text{CPY}} = \{000, 111\}$ with $n = 3$; the ground-state manifold of a L_{CPY} -complex $\mathcal{C}_{\text{CPY}} \equiv \mathcal{C}_{L_{\text{CPY}}}$ must be two-dimensional (since $|L_{\text{CPY}}| = 2$) and characterized by the property that three distinguished atoms (the ones assigned labels by ℓ) are always forced to be in the same state,

$$\mathcal{H}_0[\mathcal{C}_{\text{CPY}}] = \text{span}\{|000, a(000)\rangle, |111, a(111)\rangle\}. \quad (12)$$

Such a complex will be one of our primitives to implement check functions for tessellated target Hilbert spaces. We will discuss a specific realization \mathcal{C}_{CPY} that requires a single ancilla in Sec. VI; that is, with $N = n = 3$ atoms the target Hilbert space \mathcal{H}_{CPY} cannot be realized, whereas with $N = 4$ it can.

As another example, consider the logical XOR-gate $w_{\text{XOR}}(x_1, x_2) = x_1 \oplus x_2$, which may be needed as a primitive for a check function like Eq. (8). We can ask for a complex \mathcal{C}_{XOR} that realizes the target Hilbert space $\mathcal{H}_{\text{XOR}} = \mathcal{H}(L_{\text{XOR}})$ given by the language $L_{\text{XOR}} \equiv L[w_{\text{XOR}}] = \{000, 011, 101, 110\}$ that is generated by this Boolean gate. The ground-state manifold of such a complex must be spanned by four states,

$$\mathcal{H}_0[\mathcal{C}_{\text{XOR}}] = \text{span} \left\{ \begin{array}{ll} |000, a(000)\rangle, & |011, a(011)\rangle, \\ |101, a(101)\rangle, & |110, a(110)\rangle \end{array} \right\} \quad (13)$$

where the configurations of potential ancillas are determined by the configurations of the three ports. We will introduce a specific realization \mathcal{C}_{XOR} in Sec. VII; it requires $N = 7$ atoms of which four are ancillas, and we show that this is indeed the smallest complex that can realize the language of a XOR-gate.

Since $L_{\text{XOR}} = L[w_{\text{XOR}}]$ is generated from a Boolean gate, we refer to complexes that realize a language of this form as *gates*, too. Furthermore, we denote the atoms that map to the input bits of the gate as *input ports*, and the atom that corresponds to the output bit as the *output port*. We also extend this nomenclature to Boolean functions w on more than two inputs. Let us stress that these terms are only inspired from the usual role played by such functions as parts of Boolean circuits. In the present context, there is *no* time evolution or dynamics involved (there is no information “flowing into” the input ports, although it might be sometimes helpful to use this picture).

The construction of an L complex for a given language L with word length n can be split into two steps: First, one has to find a *structure* \mathcal{C} on at least n atoms with an $|L|$ -fold degenerate ground-state manifold. Then, one has to identify a labeling ℓ of n atoms such that their states in the ground-state manifold map one-to-one to words in L . The structure \mathcal{C} together with the labeling then yields an L complex. Note that the same structure can be interpreted as different complexes for different languages by choosing different label functions. Furthermore, not every structure with $|L|$ -fold degenerate ground-state manifold allows for a valid labeling that realizes L . Hence the construction is a quite nontrivial task in general. This makes a reductionist approach seem most promising, where one starts with a finite set of small “primitive” complexes and constructs larger complexes by “gluing” them together.

B. Amalgamation

The process of combining two complexes by joining (some of) their ports is referred to *amalgamation*. To define the process formally, we first need a new concept to combine two languages.

Consider two uniform languages L_1 and L_2 of words of length n_1 and n_2 , respectively. Let $\gamma \subseteq \{(p_1, p_2) \mid p_i \in \{1, \dots, n_i\}\}$ be a set of disjoint [60] pairs of letter positions and set $\gamma_i := \{p_i \mid p \in \gamma\}$. For a word $\mathbf{x} \in L_i$, let \mathbf{x}^{γ_i} denote the word with all letters at positions in γ_i deleted. Then, the γ

intersection of L_1 and L_2 is defined as

$$L_1 \overset{\gamma}{\cap} L_2 := \{\mathbf{x} \mathbf{y}^{\gamma_2} \mid \mathbf{x} \in L_1, \mathbf{y} \in L_2, \forall_{(a,b) \in \gamma} x_a = y_b\},$$

which is a language of words of length $n_1 + n_2 - |\gamma|$. $L_1 \overset{\gamma}{\cap} L_2$ is the set of concatenations of words from L_1 and L_2 where the letters at the positions indicated by pairs in γ coincide, and where the second copy of these letters has been deleted. Analogously, we define the *reduced γ intersection* as

$$L_1 \overset{\gamma}{\cap} L_2 := \{\mathbf{x}^{\gamma_1} \mathbf{y}^{\gamma_2} \mid \mathbf{x} \in L_1, \mathbf{y} \in L_2, \forall_{(a,b) \in \gamma} x_a = y_b\},$$

only that now *both* copies of identified letters are deleted; hence this is a language of words with length $n_1 + n_2 - 2|\gamma|$.

As an example, consider again the XOR-language $L_{\text{XOR}} = \{000, 011, 101, 110\}$ and the CPY-language $L_{\text{CPY}} = \{000, 111\}$. We would like to copy the output of the XOR-gate. To do this, we intersect the output bit (letter 3) of the XOR-language with one of the bits (say letter 1) of the CPY-language: $\gamma = \{(3, 1)\}$. The γ intersection is the new language

$$L_{\text{XOR}} \overset{\gamma}{\cap} L_{\text{CPY}} = \{00000, 01111, 10111, 11000\} \quad (14)$$

with words of length $3 + 3 - 1 = 5$. The underscores indicate the letters that derive from words of both languages. If one drops these letters as well (by using the reduced γ intersection), the language describes a XOR-gate with *fan-out* of two,

$$L_{\text{XOR}} \overset{\gamma}{\cap} L_{\text{CPY}} = \{0000, 0111, 1011, 1100\}. \quad (15)$$

The above definitions on the level of languages are useful because they are paralleled by a combination of complexes called *amalgamation*: Consider two complexes \mathcal{C}_{L_1} and \mathcal{C}_{L_2} that realize the languages L_1 and L_2 with N_1 and N_2 atoms, respectively. Fix a set of pairs of ports γ such that $L' = L_1 \overset{\gamma}{\cap} L_2 \neq \emptyset$, and then combine the two complexes by identifying the atoms in γ ,

$$\begin{aligned} \mathcal{C}_{L'} = \mathcal{C}_{L_1} \overset{\gamma}{\otimes} \mathcal{C}_{L_2} &:= \text{Diagram showing two complexes } \mathcal{C}_{L_1} \text{ and } \mathcal{C}_{L_2} \text{ with ports } \gamma \text{ identified.} \\ &= \text{Diagram showing the resulting complex } \mathcal{C}_{L'} \text{ with } N_1 + N_2 - |\gamma| \text{ atoms.} \end{aligned} \quad (16)$$

The new complex $\mathcal{C}_{L'}$ has $N_1 + N_2 - |\gamma|$ atoms. For this construction, we assume that the ports that belong to pairs in γ are located on the boundary of their complex (we will show in Sec. VI why this is possible). The Hamiltonian of the new complex is

$$H[\mathcal{C}_{L'}] = (H[\mathcal{C}_{L_1}] + H[\mathcal{C}_{L_2}] + \delta H) / \gamma, \quad (17)$$

where the formal quotient \bullet / γ indicates that pairs of atoms in γ are identified; δH denotes additional interactions between the two subcomplexes \mathcal{C}_{L_i} that vanish in the PXP model (in the vdW model they are finite but strongly suppressed due to the quick decay of U_{vdW}).

In a nutshell, $H[\mathcal{C}_{L'}]$ is the sum of the Hamiltonians of the original two complexes were the detunings of the ports that are identified by γ add up. For example, let $n^{(1)}$ and $n^{(2)}$ describe ports of \mathcal{C}_{L_1} and \mathcal{C}_{L_2} , respectively, and let γ identify

these two ports. Then $H[\mathcal{C}_{L_1}]$ contains a term $-\Delta^{(1)}n^{(1)}$ and $H[\mathcal{C}_{L_2}]$ contains a term $-\Delta^{(2)}n^{(2)}$. The Hamiltonian (17) of the amalgamation contains the term $(-\Delta^{(1)}n^{(1)} - \Delta^{(2)}n^{(2)})/\gamma = -(\Delta^{(1)} + \Delta^{(2)})n'$ where $n' = n^{(1)}/\gamma = n^{(2)}/\gamma$ describes the atom that corresponds to the identification of the two ports.

With $\delta H = 0$, it is straightforward to verify that the amalgamation $\mathcal{C}_{L'}$ realizes the language $L' = L_1 \overset{\gamma}{\cap} L_2$. This is so because the ground-state energy of $H[\mathcal{C}_{L'}]$ is lower bounded by the sum of the ground-state energies of the summands $H[\mathcal{C}_{L_i}]$; but this lower bound is realized by configurations in $L' \neq \emptyset$. The ports identified by γ can be interpreted as ancillas of the new complex if $|L_1 \overset{\gamma}{\cap} L_2| = |L_1 \overset{\gamma}{\cap} L_2|$, i.e., if the states of these atoms provide redundant information about the ground-state manifold; in this case, one would define $L' = L_1 \overset{\gamma}{\cap} L_2$ instead.

An important special case of the above construction is the amalgamation of *gates* where the input ports of one gate are identified with the output ports of others. For example, let $w(x_1, x_2)$ and $w'(x'_1, x'_2)$ be two Boolean gates that are concatenated into the circuit on three inputs $\tilde{w}(x'_1, x_1, x_2) := w'(x'_1, w(x_1, x_2))$. It is easy to see that $L[\tilde{w}] = L[w] \overset{\gamma}{\cap} L[w']$ with $\gamma = \{(3, 2)\}$ where 3 labels the third letter of words in $L[w]$, which encodes the output $y = w(x_1, x_2)$, and 2 labels the second letter of words in $L[w']$, which encodes the input x'_2 . Note that for Boolean circuits without redundancies it is always $|L[w] \overset{\gamma}{\cap} L[w']| = |L[w] \overset{\gamma}{\cap} L[w']|$ because all words are identified by the input bits. This example demonstrates that the amalgamation of gates is a crucial ingredient for the decomposition of complex Boolean circuits into a small set of simple gates.

VI. FUNCTIONAL COMPLETENESS

We have now all concepts and tools in place to formulate the main result of this paper:

Theorem 1 (Functional completeness). For every tessellated target Hilbert space $\mathcal{H}_T = \mathcal{H}_{\mathcal{L}}[f_T]$ on some lattice \mathcal{L} that is generated by a check function f_T , there exists a structure \mathcal{C}_T in the PXP model such that

$$\mathcal{H}_T \overset{\text{loc}}{\simeq} \mathcal{H}_0[\mathcal{C}_T], \quad (18)$$

with finite gap $\Delta E > 0$ and perfect degeneracy $\delta E = 0$.

In Eq. (18), $\overset{\text{loc}}{\simeq}$ denotes an isomorphism of Hilbert spaces like Eq. (11) that in addition preserves the locality structure: It maps local unitaries on \mathcal{H}_T to local unitaries on $\mathcal{H}_0[\mathcal{C}_T]$ and vice versa. Here the locality structure of $\mathcal{H}_0[\mathcal{C}_T]$ is induced by the locality structure of \mathcal{H} , which reflects the physical realization of the system. The locality structure of $\mathcal{H}_T = \mathcal{H}_{\mathcal{L}}[f_T]$ derives from the lattice \mathcal{L} and the bit-projector u_s that was used to define the tessellated language $L_{\mathcal{L}}[f_T]$; it is therefore part of the defining properties of the Hilbert space \mathcal{H}_T . This local isomorphism will be explicit for the examples in Sec. IX.

Proof. The proof of Theorem 1 is constructive in principle and best split into several steps: Steps 1 to 4 deal with the construction of a Rydberg complex $\mathcal{C}_{f_T=1}$ that implements the constraint of the check function on a single site of the lattice.

In the final Step 5, the structure \mathcal{C}_T is then constructed as the amalgamation of copies of $\mathcal{C}_{f_T=1}$ on the full lattice.

Step 1: Decomposition of f_T . The first goal is to convert the check function $f_T : \mathbb{F}_2^g \rightarrow \mathbb{F}_2$ on g binary inputs into a finite set of Boolean gates as “building blocks.” There are many universal gate sets to choose from [61] but the one that is most natural to the Rydberg platform is the singleton {NOR} that contains only the NOR-gate [62],

$$A \downarrow B := \overline{A \vee B}. \quad (19)$$

The idea behind this choice is simple: Placing three atoms A, C, B in a row such that the pairs (A, C) and (C, B) are in blockade but the pair (A, B) is not naturally gives rise to a constraint akin to $C = A \downarrow B$ (we discuss the details below). The functional completeness of {NOR} allows us to write

$$f_T(x_1, \dots, x_g) = (\dots (x_i \downarrow x_j) \dots (x_k \downarrow x_l) \dots), \quad (20)$$

where the expression on the right can be any (recursive) combination of expressions built from the input variables paired by NOR-gates. On an abstract level, this is a neat result; however, in reality one has to be more careful because variables can be used multiple times at different locations in the NOR-expansion of f_T .

To identify the true physical building blocks needed to cast Eq. (20) into a structure of atoms, it is advisable to translate the NOR-expansion into a graph G_{f_T} that represents the underlying Boolean circuit and uses the inputs x_i only *once* at dedicated “input vertices” and outputs the result $f_T(x_1, \dots, x_g)$ at a dedicated “output vertex” [Fig. 4(a)]. Otherwise, G_{f_T} is a trivalent graph with two types of vertices, corresponding to CPY-operations that copy a bit and NOR-gates that combine two bits according to Eq. (19). If we assign arrows to the edges to highlight the information flow, the two vertices are distinguished by the number of in- and outgoing edges (CPY: 1 in and 2 out, NOR: 2 in and 1 out). Furthermore, we can interpret the edges themselves as trivial single-bit gates (“LNK-gates”). If we assign Boolean values to the inputs and outputs of these three primitives according to the truth tables in Fig. 4(b), the value of the output vertex is given by $y = f_T(x_1, \dots, x_g)$. Without loss of generality, we consider only circuits without redundancy, i.e., for a given input $\{x_1, \dots, x_g\}$ the state of the inputs and outputs of all its primitives is uniquely determined. This implies that there are exactly 2^g such assignments that are parametrized by the g inputs $\{x_1, \dots, x_g\}$ (this can be seen as a *boundary* condition; in a dynamical circuit, one would call it an *initial* condition).

Step 2: Embedding of G_{f_T} . The graph G_{f_T} represents the Boolean circuit of f_T on an abstract level (only the connectivity of G_{f_T} is relevant). Our final goal is to translate this graph into a functionally equivalent structure of atoms *in the plane*. Thus we have to find an embedding $\Gamma(G_{f_T})$ of G_{f_T} in \mathbb{R}^2 ; this embedding should be planar, i.e., without crossing edges to avoid unwanted interactions. Here we skip a formal definition of $\Gamma(G_{f_T})$ and appeal to the intuition of the reader: $\Gamma(G_{f_T})$ describes a drawing of G_{f_T} in the plane without crossing edges and with well-separated vertices [Fig. 4(c)]. Of course not every graph G_{f_T} is planar, i.e., can be drawn without crossing edges in the plane. However, it has been shown long ago that every Boolean circuit can be made planar by augmenting it

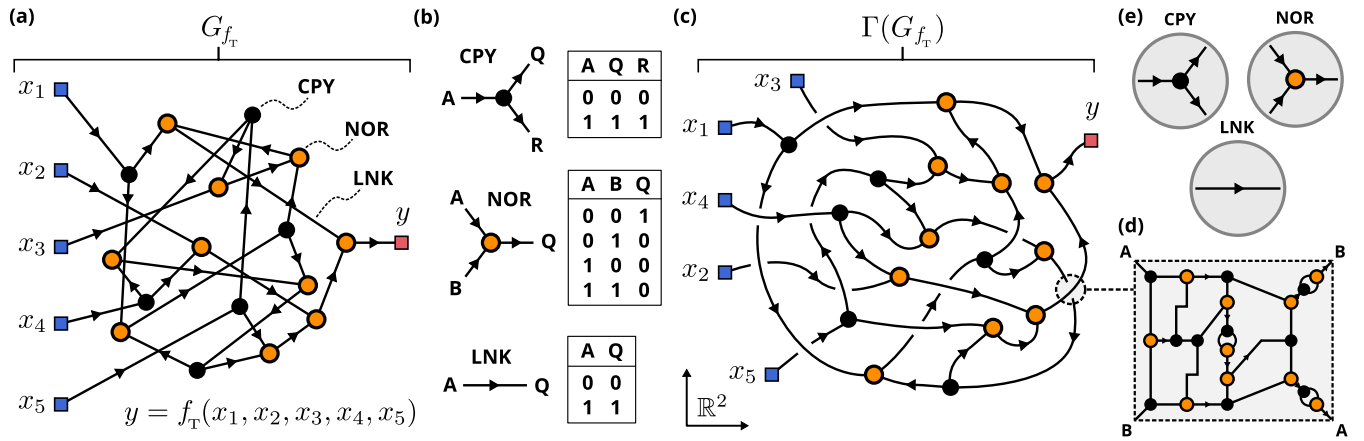


FIG. 4. Decomposition of Boolean functions. (a) Any Boolean function f_T can be represented by a graph G_{f_T} (“Boolean circuit”) with dedicated input vertices (blue squares), one output vertex (red square), and trivalent vertices (circles) of two types (b): NOR-gates with two incoming and one outgoing edge (orange circles) and CPY-vertices with one incoming and two outgoing edges (black circles); the edges themselves can be interpreted as trivial single-bit gates, here referred to as LNK-gates (black edges). If the inputs (A,B) and outputs (Q,R) of all three primitives are assigned Boolean values that satisfy the truth tables in (b), the value at the output vertex is $y = f_T(x_1, \dots)$ by construction. (c) The embedding $\Gamma(G_{f_T})$ (“drawing”) of the abstract graph G_{f_T} in the plane \mathbb{R}^2 typically involves crossings (whenever G_{f_T} is nonplanar); furthermore, input and output vertices may lie in the interior of the graph. Since a crossing of wires can be implemented with the available vertices (d), the graph can always be enhanced such that it becomes planar and input/output vertices lie on the perimeter of the embedding. (e) Locally, the embedding $\Gamma(G_{f_T})$ decomposes into three primitives, namely the structures referred to as NOR, CPY, and LNK that are functionally defined by the truth tables in (b) and geometrically by the sketches in (e).

with “crossover subcircuits” whenever two lines cross [63]. This crossover can be constructed with various gate sets, including the NOR-singleton [Fig. 4(d)]. The embedding of the crossover then uses only the three available primitives in Fig. 4(b) so that we can, without loss of generality, assume $\Gamma(G_{f_T})$ to be planar. Note that the existence of a crossover also implies that we can assume the input and output vertices to be located on the perimeter of the embedding [as realized in Fig. 4(c)]. Translated into complexes, this will prove our claim in Sec. V A that we can assume the ports to sit on the perimeter of a complex.

While $\Gamma(G_{f_T})$ may look very convoluted on a larger scale, locally it decomposes into the three simple primitives depicted in Fig. 4(e), namely CPY, NOR, and LNK. The next step is then to implement these three primitives as complexes both geometrically [i.e., following the geometry in Fig. 4(e)] and functionally [i.e., following the truth tables in Fig. 4(b)]. An f_T complex can then be obtained by amalgamation of these primitives according to the geometric blueprint provided by $\Gamma(G_{f_T})$.

Step 3a: Implementing the LNK-complex. The LNK-complex is the physical counterpart of the “wires” in the drawing of the circuit $\Gamma(G_{f_T})$. Logically, it corresponds to the trivial gate $w(x) = x$ with language $L_{\text{LNK}} = \{00, 11\}$. On the level of pure Boolean logic, wires are not entities of their own but on the physical level, sending a bit from one location to another requires dedicated machinery.

Before we discuss its construction, it is useful to introduce a more fundamental complex that can be used to construct two of the three primitives: the NOT-gate with defining language $L_- = \{01, 10\}$; it realizes the single-bit gate $w(x) = \bar{x}$ and formalizes the core concept of the Rydberg blockade. In the PXP model, it can be realized naturally without ancillas by

the Hamiltonian

$$H_- = -\Delta(n_A + n_Q) \quad (21)$$

with a complex \mathcal{C}_- where $|r_A - r_Q| < r_B$. The subscripts denote the labels of the ports assigned by ℓ (we reserve A, B, ... for input ports and Q, R, ... for output ports). The ground-state manifold is $\mathcal{H}_0[\mathcal{C}_-] = \text{span}\{|01\rangle, |10\rangle\}$ with degeneracy $\delta E_- = 0$ and gap $\Delta E_- = \Delta > 0$.

The elementary LNK-complex that translates a bit in space can then be constructed as the amalgamation of two NOT-gates [Fig. 5(a)] with Hamiltonian

$$H_{\text{LNK}} = -\Delta n_A - 2\Delta \tilde{n}_1 - \Delta n_Q, \quad (22)$$

where adjacent atoms are in blockade but next-nearest neighbors are not. Above and in the following we label ancillas with a tilde and assign them numerical indices. As for the NOT-gate, it is $\delta E_{\text{LNK}} = 0$ and $\Delta E_{\text{LNK}} = \Delta$ with the LNK-manifold

$$\mathcal{H}_0[\mathcal{C}_{\text{LNK}}] = \text{span}\{|0(1)0\rangle, |1(0)1\rangle\}. \quad (23)$$

Here and in the following we mark the states of ancillas by parentheses. Repeated amalgamation of elementary LNK-complexes results in LNK-complexes of arbitrary length (always composed of an odd number of atoms and with halved detuning at the endpoints). The two states in $\mathcal{H}_0[\mathcal{C}_{\text{LNK}}]$ of such chains correspond to the two ground states of an antiferromagnetic Ising chain.

Step 3b: Implementing the CPY-complex. The purpose of the CPY-complex is to copy classical bits; it is defined by the “copy” language $L_{\text{CPY}} = \{000, 111\}$. The CPY-complex is necessary because expansions in universal gates can reuse inputs multiple times. Furthermore, circuits can be simplified dramatically if intermediate results can be reused. In conventional drawings of Boolean circuits, the possibility to copy bits

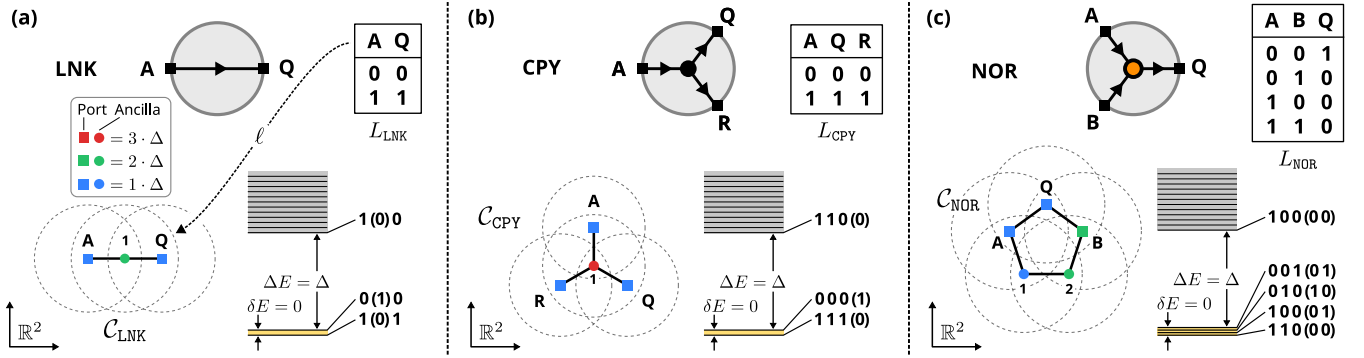


FIG. 5. Complete set of logic primitives. (a) The (elementary) LNK-complex \mathcal{C}_{LNK} can be realized by a chain of three atoms where adjacent atoms are in blockade (black edges). The detuning of the ports Δ (blue squares, labeled by ℓ) is half that of the ancilla 2Δ (green circle) in the bulk. The width δE and gap ΔE are shown together with a schematic spectrum that highlights the logical manifold $\mathcal{H}_0[\mathcal{C}_{\text{LNK}}]$ and one of the states orthogonal to $\mathcal{H}_0[\mathcal{C}_{\text{LNK}}]$ that define the gap. The state of ancillas is shown in parentheses. (b) The CPY-complex \mathcal{C}_{CPY} can be realized with a central ancilla (red circle) that is in blockade with the three surrounding atoms (blue squares). To make the two logical states degenerate, the ancilla has a detuning of 3Δ if the other atoms are detuned by Δ . (c) The NOR-complex \mathcal{C}_{NOR} can be realized with two ancillas (blue and green circles) that form a ring-like blockade with the three ports (blue and green squares). To make the four logical states unique and degenerate, the detunings cannot be chosen uniformly but must break the reflection symmetry about the axis through the output port Q .

is silently assumed whenever one splits up wires. Again, in a physical implementation one has to provide the means to do so.

The implementation of the CPY-complex is detailed in Fig. 5(b). It is easy to see (Appendix A 1) that there cannot be a CPY-complex without ancillas because the configuration 111 excludes a Rydberg blockade between any of the three ports (which would automatically render them completely uncorrelated). Adding a single ancilla does the trick because the amalgamation of three NOT-complexes on a single atom yields the desired complex by construction. The four atoms are described by the Hamiltonian

$$H_{\text{CPY}} = -\Delta(n_A + n_Q + n_R) - 3\Delta \tilde{n}_1, \quad (24)$$

and the geometry of the complex \mathcal{C}_{CPY} is chosen so that the ancilla is in blockade with the three ports, but these are not within blockade of each other. In combination with Eq. (24), this implements the CPY-manifold,

$$\mathcal{H}_0[\mathcal{C}_{\text{CPY}}] = \text{span} \{ |000(1)\rangle, |111(0)\rangle \} \quad (25)$$

with $\delta E_{\text{CPY}} = 0$ and $\Delta E_{\text{CPY}} = \Delta > 0$.

Step 3c: Implementing the NOR-complex. The NOR-complex is crucial as it realizes a functionally complete two-bit gate; it is specified by the language $L_{\text{NOR}} = \{001, 010, 100, 110\}$. In contrast to the LNK- and CPY-complexes, the NOR-complex cannot be bootstrapped from the NOT-complex but must be constructed from scratch.

In Appendix A 2 we show that a NOR-complex cannot be realized with less than two ancillas in the PXP model. One implementation of a NOR-complex is detailed in Fig. 5(c). The five atoms are governed by the Hamiltonian

$$H_{\text{NOR}} = -\Delta(n_A + n_Q + \tilde{n}_1) - 2\Delta(n_B + \tilde{n}_2), \quad (26)$$

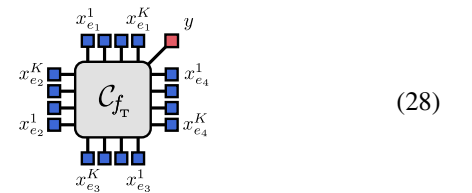
which gives rise to the NOR-manifold

$$\mathcal{H}_0[\mathcal{C}_{\text{NOR}}] = \text{span} \left\{ \begin{array}{l} |001(01)\rangle, |010(10)\rangle, \\ |100(01)\rangle, |110(00)\rangle \end{array} \right\} \quad (27)$$

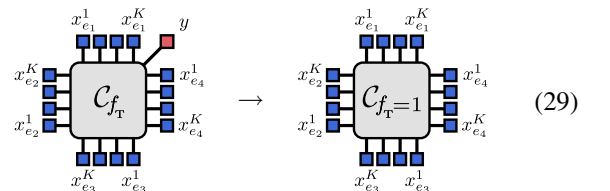
with $\delta E_{\text{NOR}} = 0$ and $\Delta E_{\text{NOR}} = \Delta$; this requires that the atoms are arranged in a ring-like blockade, as depicted in Fig. 5(c).

Note that the two ancillas are only necessary to enforce the degeneracy of the logical states 010 and 100 with 110. All remaining constraints come for free with the Rydberg blockade. As we will show in Sec. VII, the NOR-complex in Fig. 5(c) is not unique. We will also see that the only fundamental Boolean gate that can be realized with as few as five atoms is the NOR-gate, confirming our intuition in Step 1 that the NOR-gate is the most natural on the Rydberg platform.

Step 4: Constructing the f_T -complex. To construct a complex \mathcal{C}_{f_T} that implements the check function f_T (more precisely: the language $L[f_T]$), one combines the three primitives above according to an embedding $\Gamma(G_{f_T})$. Since all vertices are (at most) trivalent, it is easy to check that an amalgamation in the PXP model is possible without geometrical obstructions, and that this procedure yields an f_T -complex with $\delta E_{f_T} = 0$ and $\Delta E_{f_T} \geq \Delta > 0$. At this point, we have a complex with $g = 4K$ input ports on its boundary that outputs $y = f_T(x_1^1, \dots)$ on a dedicated output port (also on its boundary, but this is not important in the following),

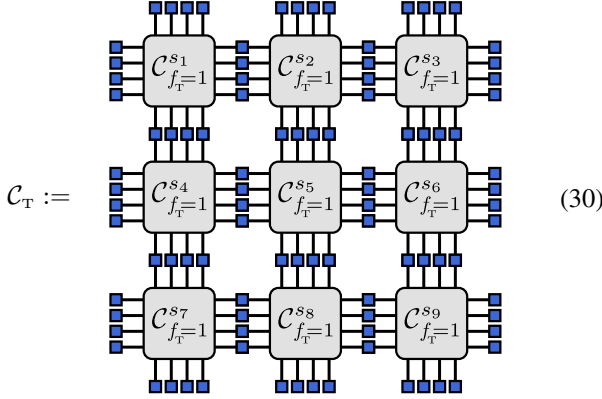


To enforce the constraint $f_T(x_1^1, \dots) \stackrel{!}{=} 1$, we only have to add a local detuning on the output port to lower the energy of valid configurations and gap out invalid ones. This boils down to a simple modification of the check function complex,



where the output port is detuned and downgraded to an ancilla. The ground-state manifold of the modified complex $\mathcal{C}_{f_T=1}$ consists of all input configurations for which $f_T(x_{e_1}^1, \dots) = 1$.

Step 5: Constructing \mathcal{C}_T . The complex $\mathcal{C}_{f_T=1}$ enforces the local constraint of the check function on a single site of the lattice on which the tessellated target Hilbert space $\mathcal{H}_T = \mathcal{H}_{\mathcal{L}}[f_T]$ is defined. To construct \mathcal{C}_T for the full system, place a copy $\mathcal{C}_{f_T=1} \mapsto \mathcal{C}_{f_T=1}^s$ on every site $s \in V(\mathcal{L})$ of the lattice, and amalgamate adjacent complexes at the corresponding ports (possibly using LNK-complexes to avoid unwanted interactions),



By construction, the ground states of this complex are in one-to-one correspondence with words $x \in L_{\mathcal{L}}[f_T]$ (using the ports on the edges denoted by blue squares). Note that here we show the construction for a square lattice \mathcal{L} ; the generalization to other lattices is straightforward.

This concludes the construction of \mathcal{C}_T such that $\mathcal{H}_T \stackrel{\text{loc}}{\simeq} \mathcal{H}_0[\mathcal{C}_T]$ in the PXP approximation. Note that the ancillas do not introduce additional degrees of freedom in this subspace and local unitaries on \mathcal{H}_T map to local unitaries on $\mathcal{H}_0[\mathcal{C}_T]$ (the latter involve the ancillas of the $\mathcal{C}_{f_T=1}$ complexes and can therefore be very complicated—but they remain local on \mathcal{H}). ■

We conclude this section with a few remarks.

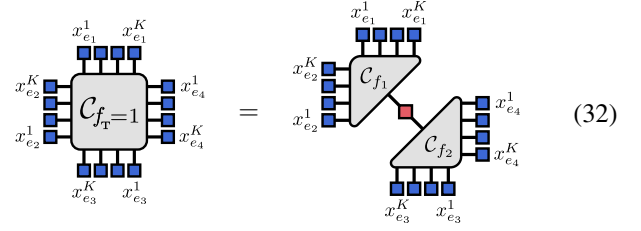
First, while the proof above *is* constructive, one should not expect the resulting structures to be useful in real-world applications, except for simple special cases. In particular, we established no claims about optimality (in any sense) of the constructed f_T -complexes; on this we focus in the next Sec. VII.

Second, the modification in Eq. (29) to construct $\mathcal{C}_{f_T=1}$ from \mathcal{C}_{f_T} is often straightforward to implement and can simplify the complex considerably: When there are no blockades between the output port and some of the input ports, one simply *deletes* the output port along with all ancillas that are in blockade with it. This removes all configurations of input ports from the ground-state manifold where the output was not excited (see Appendix B). The removal of the output port may not be necessary at all if the constraint $f_T(x_{e_1}^1, \dots) \stackrel{!}{=} 1$ can be rewritten as an equality of the form

$$f_1(x_{e_1}^1, \dots, x_{e_2}^1, \dots) \stackrel{!}{=} f_2(x_{e_3}^1, \dots, x_{e_4}^1, \dots), \quad (31)$$

with Boolean functions $f_{1,2}$ that take only $2K$ inputs each. Then $\mathcal{C}_{f_T=1} = \mathcal{C}_{f_1} \overset{\vee}{\otimes} \mathcal{C}_{f_2}$ where the two complexes are

amalgamated at their output ports,



An example for this construction can be found in Sec. IX A.

Lastly, the constructive proof implies that all Boolean functions can be realized by a complex with *bounded* detuning range $\{1\Delta, 2\Delta, 3\Delta\}$, i.e., detunings do not grow with the size (or depth) of the Boolean circuit. Indeed, since the ports of the LNK-complex have detuning 1Δ , and the ports of the CPY- and NOR-complexes at most 2Δ , amalgamations of the latter two primitives via LNK-complexes produce atoms with maximum detuning 3Δ . This result is particularly important for experimental realizations that always operate within a bounded range of applicable detunings.

VII. LOGIC PRIMITIVES

A crucial step of the proof in the previous section is to show that every Boolean function f can be realized by a Rydberg complex \mathcal{C}_f in the sense that the language $L[f]$ of its truth table can be realized as ground-state manifold. As mentioned above, the complexes that arise from the decomposition of f into LNK-, CPY- and NOR-primitives are typically large and convoluted. For example, the decomposition of a simple AND-gate (\wedge) into NOR-gates reads

$$A \wedge B = (A \downarrow A) \downarrow (B \downarrow B), \quad (33)$$

which would require two CPY- and three NOR-complexes, wired together by a bunch of LNK-complexes so that the resulting complex requires more than 20 atoms. As this is way too much overhead for a simple gate, the question arises whether important primitives of Boolean logic can be realized by complexes that are much smaller than the ones described by the NOR-decomposition in Sec. VI.

The answer is positive: In the following, we discuss provably minimal complexes for the most important gates of Boolean logic, all of which improve significantly over the naive NOR-decomposition. Besides the usual gates of Boolean algebra, NOT (\neg or \bullet), AND (\wedge), and OR (\vee), we search for minimal complexes that realize the following common logic gates (given in disjunctive normal form),

$$\text{NOR: } A \downarrow B = \overline{A \wedge B}, \quad (34a)$$

$$\text{NAND: } A \uparrow B := \overline{A \vee B}, \quad (34b)$$

$$\text{XOR: } A \oplus B := (A \wedge \overline{B}) \vee (\overline{A} \wedge B), \quad (34c)$$

$$\text{XNOR: } A \odot B := (A \wedge B) \vee (\overline{A} \wedge \overline{B}). \quad (34d)$$

Of these gates, only NOR and NAND are universal on their own. The following identities show that some of these gates are simply inverted versions of others (we will use this below):

$$A \wedge B = \overline{\overline{A} \uparrow \overline{B}}, \quad (35a)$$

$$A \vee B = \overline{\overline{A} \downarrow \overline{B}}, \quad (35b)$$

$$A \oplus B = \overline{\overline{A} \odot \overline{B}}. \quad (35c)$$

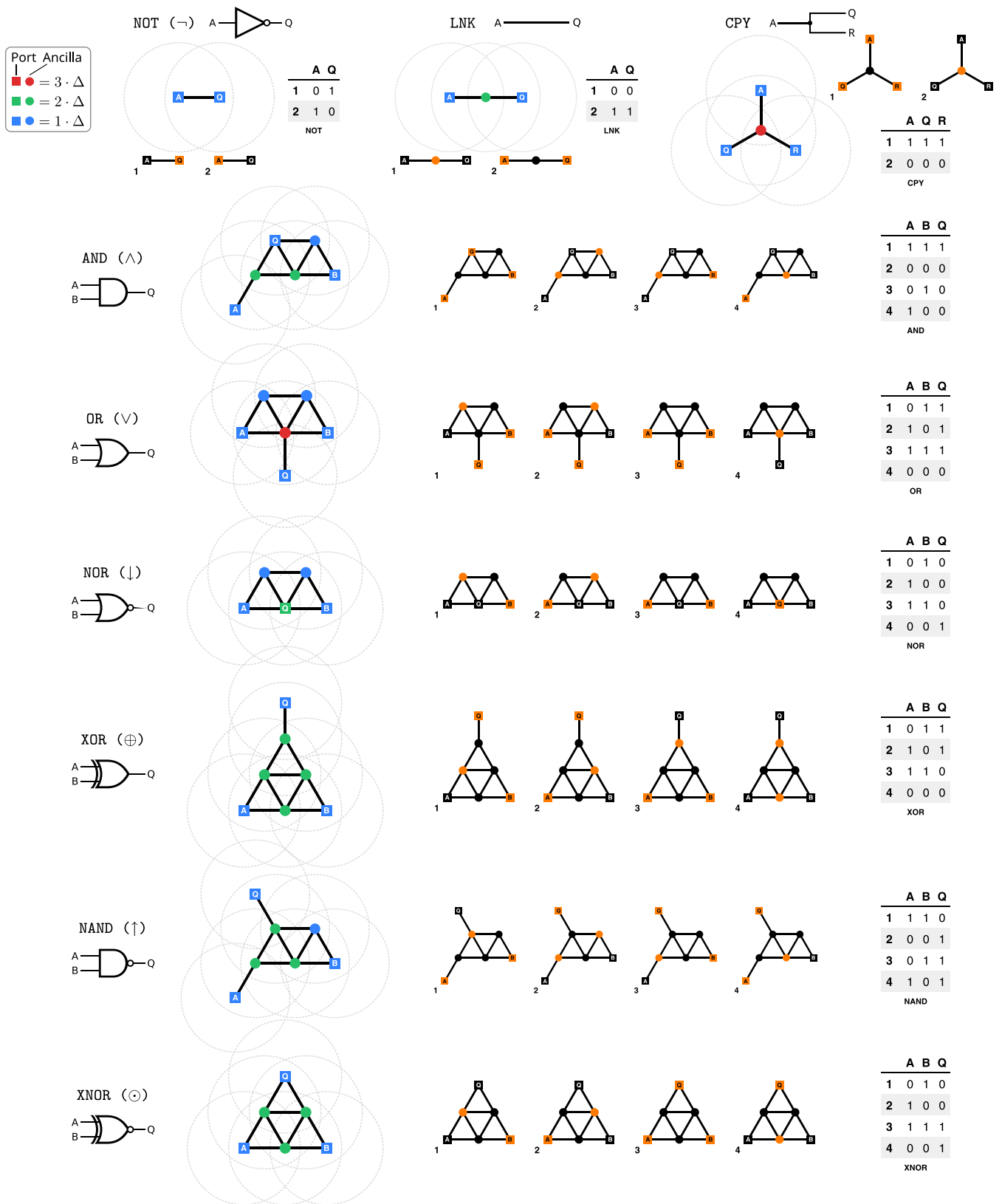


FIG. 6. Common logic primitives. Rydberg complexes for the most common primitives of Boolean circuits. All complexes are provably minimal, see Appendix A. Note that *minimal* complexes are not necessarily *unique*; e.g., the shown NOR-gate is an alternative to the one in Fig. 5(c), both of which are minimal. For each complex we show (1) the geometry with blockade radii (gray dashed circles), (2) the complete ground-state manifold (orange: $|1\rangle$, black: $|0\rangle$), and (3) the truth table of the ports (labeled atoms) in the ground-state manifold. The rows of the truth tables correspond to the numbered ground-state configurations. Colors of ancillas and ports in the geometry encode the detuning (see key). Atoms in blockade are connected by black solid lines.

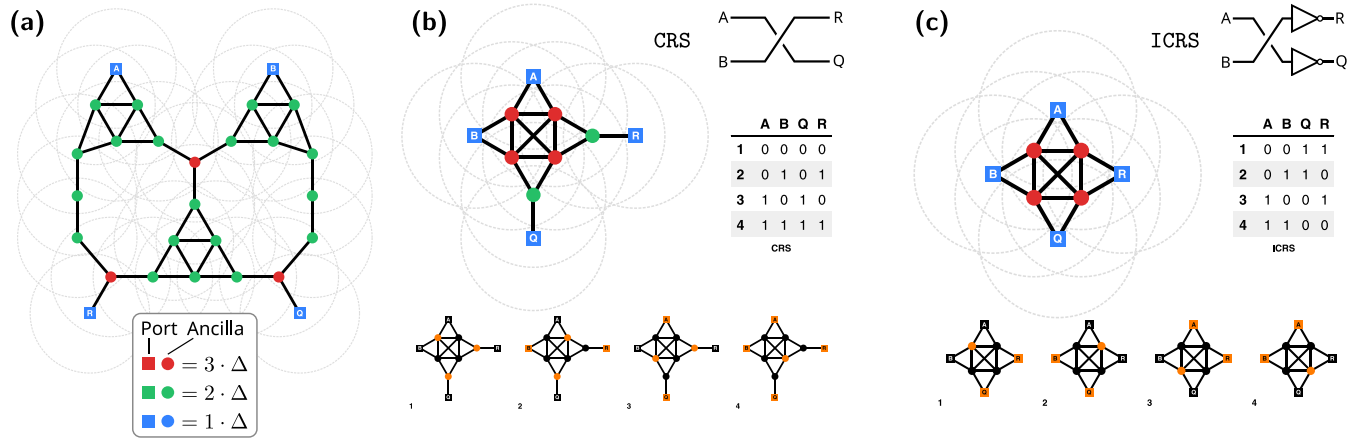


FIG. 7. Crossing. (a) The crossing constructed from the Boolean circuit crossing based on XNOR-gates (see Ref. [63] and Fig. 6); it is an amalgamation of LNK-, CPY-, and XNOR-complexes. The ground-state manifold (not shown) is fourfold degenerate and ensures $A = Q$ and $B = R$. The complex requires ~ 27 atoms and is therefore of no practical relevance. (b) By contrast, the minimal crossing C_{CRS} requires only 10 atoms; it was constructed by systematically excluding functionally equivalent complexes with fewer atoms. The shown data is explained in the caption of Fig. 6. (c) The minimal *inverted* crossing C_{ICRS} is smaller than the noninverted crossing and requires only eight atoms. To construct C_{CRS} from C_{ICRS} , two NOT-complexes must be amalgamated to adjacent ports. This is a recurring scheme due to the inverting nature of the Rydberg blockade.

Of the gates $\{\neg, \vee, \wedge, \uparrow, \downarrow, \oplus, \odot\}$, we already know minimal complexes for NOT (two atoms) and NOR (five atoms), recall Sec. VI.

Using Eq. (35b), we can immediately construct an OR-complex with six atoms by amalgamation of a NOT-complex to the output port of a NOR-complex (remember Fig. 1). However, it is unclear whether this complex is *minimal*, i.e., cannot be realized with fewer atoms. Therefore we systematically devised proofs that a given truth table *cannot* be realized with a given number N of atoms, starting at $N = 3$ for each gate, and increasing the number incrementally until the proof fails, i.e., realizations can no longer be excluded. These arguments are quite technical and can be found in Appendix A. However, this approach has two benefits: First, it provides rigorous lower bounds on how many atoms are needed to realize a given gate, and second, it often provides a blueprint for the construction of a minimal complex that saturates this bound by carefully observing *why* one cannot exclude realizations with a given number of atoms.

To complement this rigorous approach, we conducted a brute force search on a computer that exhaustively scans for (small) complexes that realize a given truth table. In accordance with our proofs, we found solutions with the minimal atom number for a given truth table (in addition, we also found nonminimal complexes). Interestingly, there were alternative minimal solutions that we missed in our manual approach; so minimal complexes are not necessarily unique.

A selection of provably minimal complexes for all important Boolean primitives is shown in Fig. 6 (for the sake of completeness, we include the NOT-, LNK- and CPY-complexes discussed in Sec. VI). There are a few comments in order. First, an example of nonunique minimal complexes is the depicted NOR-complex built from five atoms arranged in a triangular structure [cf. the ring-shaped structure in Fig. 5(c)]. Second, the six-atom OR-complex we proposed above indeed is minimal, although not unique either. Third, the selection

of minimal complexes in Fig. 6 for $\{\vee, \wedge, \uparrow, \downarrow, \oplus, \odot\}$ all build around the triangle-based core of the NOR-complex, once again emphasizing its central role in the context of Rydberg complexes. Finally, it turns out that the relations (35) are all reflected in the minimal complexes, e.g., the amalgamation of a NOT-complex and a XNOR-complex yields a minimal XOR-complex; similar constructions hold for NAND and AND as well as NOR and OR. If we recall the relation between NOT and the minimal LNK-complex, the general picture emerges that inverting complexes are simpler (by one atom) than noninverting ones. This is understandable in so far as inversion is the most basic operation the Rydberg blockade is capable of, thus leading to the simplest complexes. This is in contrast to the notation for Boolean circuits known from electrical engineering where inverting gates are represented by more complicated symbols than their noninverting counterparts (Fig. 6).

VIII. CROSSING

The crossing complex realizes the somewhat surprising feature of intersecting information channels in a strictly two-dimensional setup of strongly interacting information carriers (recall Step 2 in Sec. VI). The possibility to realize such a planar crossing in a circuit with the three primitives LNK, CPY, and NOR was crucial for the proof of Theorem 1. Note that the *existence* of such a complex followed immediately from the existence of the three aforementioned complexes and the well-known fact that Boolean circuits can be made planar [63]. However, just as for the Boolean gates in Sec. VII, the NOR-based implementation of the circuit crossing in Ref. [63] is of low practical value as it requires seven NOR-gates [if we implement NOT-gates directly, Fig. 4(d)]; even a simpler crossing based on only three minimal XNOR-gates requires ~ 27 atoms, see Fig. 7(a). Thus we are again tasked with finding a minimal complex that realizes the same function.

By systematically excluding the existence of crossing complexes for $N = 4, \dots, 9$ atoms, we finally find the minimal complex \mathcal{C}_{CRS} depicted in Fig. 7(b) comprising 10 atoms. The proof for its minimality is very technical and more complicated than for the logic primitives because geometric constraints must be taken into account for the crossing [64]. The structure with two dangling ports (Q and R) immediately suggests the *inverted* crossing $\mathcal{C}_{\text{ICRS}}$ in Fig. 7(c) with eight atoms, i.e., a complex that allows two signals to pass each other while inverting both at the same time. The minimality of the inverted crossing complex $\mathcal{C}_{\text{ICRS}}$ with eight atoms follows as a corollary from the minimality of the noninverted crossing \mathcal{C}_{CRS} with 10 atoms as the latter can be obtained from the former by amalgamation of two NOT-complexes (thereby adding two atoms). In line with our comment at the end of the previous Sec. VII, the inverted variant of the crossing is smaller than its noninverted counterpart. We note that the inverted crossing $\mathcal{C}_{\text{ICRS}}$ has also been described in Ref. [33] where it plays an important role in mapping nonplanar optimization problems to planar Rydberg structures.

IX. EXAMPLES: SPIN LIQUID PRIMITIVES

In this part, we focus on our motivation outlined in the introduction, namely the implementation of tessellated target Hilbert spaces of systems that are characterized by local gauge constraints. We discuss two models exemplarily: the surface code with Abelian \mathbb{Z}_2 topological order and the non-Abelian Fibonacci model. For the surface code, we will be able to utilize the Boolean primitives discussed in Sec. VII; by contrast, for the Fibonacci model such a reduction will not be useful.

A. Surface code

The *toric code* [47] is the prime example for a spin liquid in two dimensions with long-range entangled ground states that do not break any symmetries but instead feature *topological order*. The toric code is referred to as *surface code* if realized on surfaces with boundaries [65]; we will stick to this name in the following. The surface code describes a gapped phase with \mathbb{Z}_2 topological order that is described by the mechanism of string-net condensation [48]. It allows for localized excitations that are Abelian anyons [66], which, in turn, leads to ground-state degeneracies on topologically nontrivial surfaces (including flat surfaces with nontrivial boundaries). As a consequence, surface codes are promising candidates for quantum memories that encode logical qubits reliably into delocalized degrees of freedom [67]. This makes the implementation of systems with this kind of topological order interesting both from an academic and an applied perspective [44,68,69].

Here we consider the surface code on a finite square lattice with “rough” boundaries [like the gray background lattice in Fig. 8(d)]; “rough” boundaries are terminated by dangling edges that attach to quadrivalent vertices. The Hamiltonian

$$H = -J_A \sum_{\text{Sites } s} A_s - J_B \sum_{\text{Faces } p} B_p \quad (36)$$

operates on qubits that live on the edges e of the square lattice. The operators

$$A_s = \prod_{e \in s} \sigma_e^z \quad \text{and} \quad B_p = \prod_{e \in p} \sigma_e^x \quad (37)$$

are referred to as *star* and *plaquette* operators, respectively. Here, $e \in s$ denotes edges that emanate from site s and $e \in p$ denotes sites that bound face p ; σ_e^α are Pauli matrices for $\alpha = x, y, z$ acting on the qubit on edge e . Since $[A_s, B_p] = 0$, the Hamiltonian (36) is frustration-free and its ground state $|G\rangle$ is characterized by $A_s|G\rangle = B_p|G\rangle = |G\rangle$ for all sites s and faces p (assuming $J_A, J_B > 0$). Due to the uniform “rough” boundaries there is no ground-state degeneracy and $|G\rangle$ is unique.

The construction of $|G\rangle$ is straightforward: To satisfy the constraint $A_s|G\rangle = |G\rangle$ on sites s , one can choose the product state $|\mathbf{0}\rangle$ with $\sigma_e^z|\mathbf{0}\rangle = |\mathbf{0}\rangle$ for all edges. This state does *not* satisfy the constraint $B_p|G\rangle = |G\rangle$ on faces, though. To fix this, one defines the multiplicative group $\mathcal{B} = \langle \{B_p | \text{Faces } p\} \rangle$ generated by all plaquette operators (note that $B_p^2 = \mathbb{1}$), and constructs the superposition

$$|G\rangle \propto \sum_{C \in \mathcal{B}} C|\mathbf{0}\rangle. \quad (38)$$

The state $|G\rangle$ is invariant under any B_p by construction since \mathcal{B} is left-invariant under any B_p by definition. Furthermore, since $[A_s, B_p] = 0$, the site-constraint $A_s|G\rangle = |G\rangle$ is still satisfied. Thus Eq. (38) describes, up to normalization, the unique ground state of Eq. (36).

The states $|C\rangle \equiv C|\mathbf{0}\rangle$ have a peculiar structure: Each C can be described as a collection of closed loops on the lattice where the σ_e^x of products of B_p operators act (loops that terminate on dangling edges at the boundary are considered closed); this loop structure is then imprinted on $|\mathbf{0}\rangle$ so that $|C\rangle$ is a product state with a loop pattern C of flipped qubits $|1\rangle$. The ground state Eq. (38) is therefore given by the equal-weight superposition of all closed loop configurations on the square lattice—which makes it an example of a *string-net condensate* [48] with a nontrivial pattern of long-range entanglement [70,71].

To prepare this state in a real system, one could try to implement the Hamiltonian (36) and cool the system into its ground state. This is a challenging task due to the four-body interactions (37), which are notoriously hard to realize. On the Rydberg platform, an alternative and more promising approach goes as follows: In a first step, one prepares only the subspace

$$\begin{aligned} \mathcal{H}_{\text{Loop}} &:= \{|\Psi\rangle | \forall \text{ Sites } s : A_s|\Psi\rangle = |\Psi\rangle\} \\ &= \text{span} \{|C\rangle | C \in \mathcal{B}\} \end{aligned} \quad (39)$$

as the low-energy manifold of a suitably designed structure of atoms. ($\mathcal{H}_{\text{Loop}}$ is the Hilbert space of a \mathbb{Z}_2 lattice gauge theory with charge-free background [59]. The local constraint $A_s|\Psi\rangle = |\Psi\rangle$ corresponds to the gauge symmetry of this theory and is known as *Gauss’s law*.) The B_p terms in Eq. (36) induce quantum fluctuations on this subspace, which give rise to the string-net condensed ground state in Eq. (38). On the Rydberg platform, quantum fluctuations can be induced *perturbatively* by ramping up the Rabi frequency Ω_i . Such fluctuations can give rise to interesting quantum phases, as shown in Ref. [41] for a different model. This motivates the

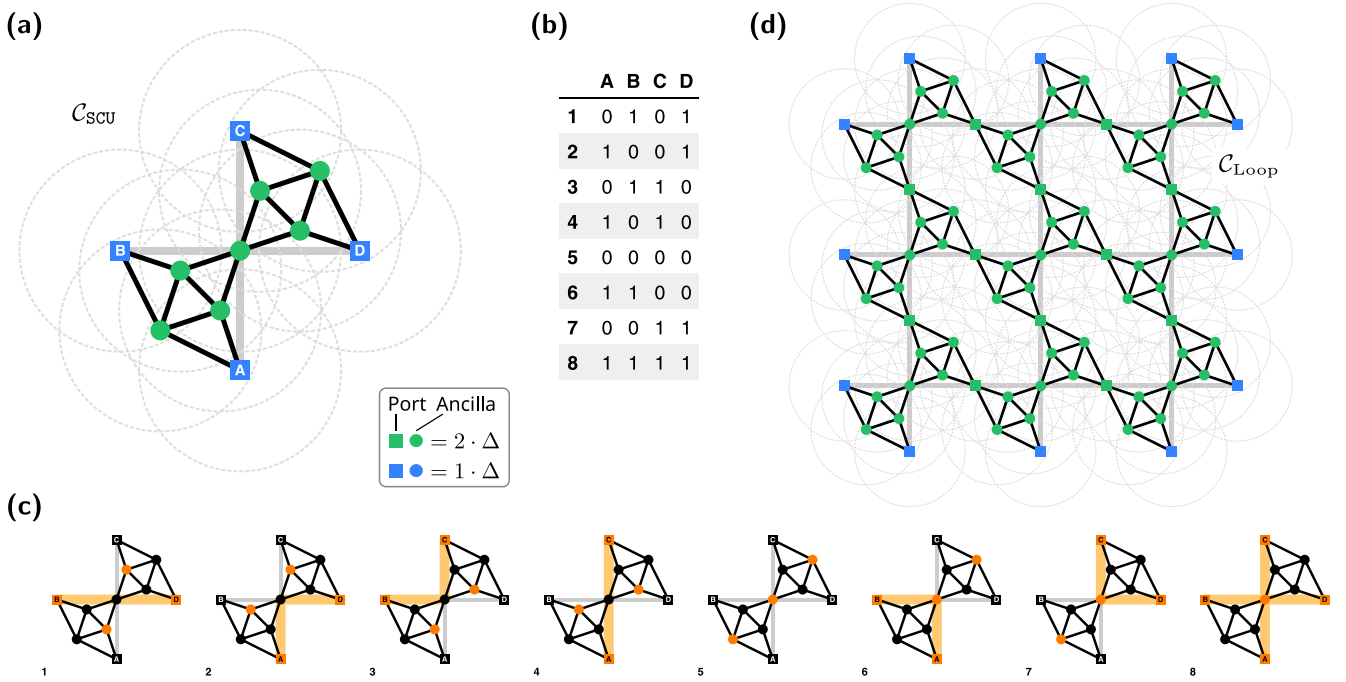


FIG. 8. Surface code. (a) Unit-cell/vertex complex \mathcal{C}_{SCU} for the surface code (\mathbb{Z}_2 topological order). The complex is the amalgamation and deformation of two XNOR-complexes [see Fig. 6 and Eq. (43)] and implements the check function constraint $f_{\text{Loop}} = 1$ defined in Eq. (42). The deformations are necessary to prevent an unwanted blockade of ancillas in the amalgamation. Black edges denote blockades between atoms, gray edges illustrate the underlying square lattice. [(b), (c)] Truth table and ground-state manifold of the complex. The manifold contains all configurations with an even number of labeled atoms excited, thereby realizing Gauss’s law on the site (colored edges). This provides the local isomorphism between $\mathcal{H}_T = \mathcal{H}_{\text{Loop}}$ and $\mathcal{H}_0[\mathcal{C}_{\text{Loop}}]$. (d) Periodic tessellation $\mathcal{C}_{\text{Loop}}$ of the vertex complex \mathcal{C}_{SCU} . The copies overlap on the edges and are amalgamated at these ports (which makes the detunings uniform in the bulk).

construction of a Rydberg complex $\mathcal{C}_{\text{Loop}}$ with

$$\mathcal{H}_0[\mathcal{C}_{\text{Loop}}] \stackrel{\text{loc}}{\simeq} \mathcal{H}_T = \mathcal{H}_{\text{Loop}} = \text{span} \{ |C\rangle \mid C \in \mathcal{B} \}, \quad (40)$$

i.e., a Rydberg complex the degenerate ground states of which can be locally mapped one-to-one to loop configurations on the square lattice. $\mathcal{H}_0[\mathcal{C}_{\text{Loop}}]$ is then a subspace with dimension $\dim \mathcal{H}_0[\mathcal{C}_{\text{Loop}}] \sim 2^M$ where M denotes the number of unit cells of the square lattice. Note that $\mathcal{H}_0[\mathcal{C}_{\text{Loop}}]$ cannot be decomposed into factors of local Hilbert spaces [like, e.g., the full Hilbert space $\mathcal{H} = (\mathbb{C}^2)^{\otimes 2M}$ can].

To this end, we assign bits x_e^1 to the edges of the square lattice \mathcal{L} ($K = 1$). Our goal is to specify the tessellated “loop language” $\mathcal{L}_{\mathcal{L}}[f_{\text{Loop}}]$ —which contains all bit patterns that trace out closed loop configurations on the lattice (closed in the sense defined above)—in terms of a local check function f_{Loop} and a local bit-projector u_s on each site s of the square lattice. The bit-projector simply selects the four bits on edges adjacent to s ,

$$u_s \left(\begin{array}{c} \bullet \\ \bullet \\ \bullet \\ \bullet \end{array} \right) = (x_{e_1}^1, x_{e_2}^1, x_{e_3}^1, x_{e_4}^1) \quad (41)$$

and the check function reads

$$f_{\text{Loop}}(x_1, x_2, x_3, x_4) = (x_1 \odot x_2) \odot (x_3 \odot x_4) \quad (42)$$

with the XNOR-gate \odot defined in Eq. (34d), that is, $A \odot B = 1$ iff $A = B$. It is easy to verify by inspection that $f_{\text{Loop}} = 1$ if

and only if the number of active bits is *even*, thereby enforcing Gauss’s law on every site of the lattice (because loops cannot terminate there).

We could now construct a complex as discussed in Sec. V A, using the minimal XNOR-complex depicted in Fig. 6. For this construction, we would amalgamate three of these complexes according to Eq. (42) and detune the final output to enforce $f_{\text{Loop}} = 1$; this would require at least 16 atoms per site. However, we can do much better by rewriting the constraint as an equality,

$$f_{\text{Loop}} = 1 \Leftrightarrow x_1 \odot x_2 = x_3 \odot x_4. \quad (43)$$

Indeed, Eq. (43) evaluates to true iff $x_1 + x_2 + x_3 + x_4$ is even. In general, an implementation of an equality constraint $f_1 = f_2$ of two functions on separate inputs is achieved by amalgamation of their complexes \mathcal{C}_{f_1} and \mathcal{C}_{f_2} at their output ports, as noted at the end of Sec. VI. Therefore, the vertex complex $\mathcal{C}_{\text{SCU}} \equiv \mathcal{C}_{f_{\text{Loop}}=1}$ (“surface code unit cell”) that realizes the constraint Eq. (43) is that of only *two* XNOR-gates amalgamated at their outputs [Fig. 8(a)], which requires only 11 atoms. Surprisingly, it turns out that this realization is also minimal, see Appendix C 1 for a proof. (Note that typically the construction of larger complexes from minimal primitives does *not* yield minimal complexes.) The two XNOR-complexes that make up the vertex complex are geometrically deformed variants of the XNOR-complex shown in Fig. 6. This is necessary to prevent unwanted blockades between ancillas in the amalgamation.

In Fig. 8(b) we show the configurations of the four labeled ports (A, B, C, and D) of the complex in the eightfold degenerate ground-state manifold. In Fig. 8(c) we illustrate the excitation patterns of these eight ground states (atoms excited to the Rydberg state are colored orange). Highlighting the edges of the square lattice whenever the labeled ports associated to them are excited yields the local mapping (40) to the loop structure of states in $\mathcal{H}_{\text{Loop}}$. Note that the ancillas do not add additional degrees of freedom in the ground-state manifold.

For the tessellation [Fig. 8(d)] the vertex complex is copied and shifted periodically along the basis vectors of the square lattice. The labeled ports are then amalgamated to the corresponding ports of complexes on adjacent sites. Quite remarkably, due to the amalgamation, the detunings in the bulk become uniform, which makes this tessellation interesting under the constraints of current platforms [39,44]. (Note that imposing periodic boundary conditions on the lattice, i.e., going back to the *toric* code, would render the detunings completely uniform.)

Let us briefly comment on the modifications of the surface code patch in Fig. 8(d) that would be necessary to use it as a quantum code. It is well known [65] that a surface code patch encodes a single logical qubit if its four sides alternate in boundary types: top and bottom remain “rough” but left and right are modified to “smooth” boundaries by cutting of the dangling edges of the square lattice. On these boundaries, the sites become trivalent “T” shaped with the same Gauss’s law (i.e., the number of active edges must be even). On these sites, the quadrivalent complex in Fig. 8(a) must be replaced by a trivalent one. Conveniently enough, this is just the XOR-complex in Fig. 6 as the truth table of XOR contains exactly the four assignments of three Boolean variables such that $x_1 + x_2 + x_3$ is even. As a bonus, closing of the left and right sides of the patch with XOR-complexes leads to completely uniform detunings along these boundaries. The simplicity of the vertex complex on trivalent sites suggests a definition of the surface code on the Honeycomb lattice (which is perfectly possible [48]). However, because of the two sites per unit cell, this does not reduce the number of required atoms per unit cell to implement the check function. Indeed, the realizations with minimal Rydberg complexes on both lattices are essentially equivalent, as can be seen in Fig. 8(d) by rotating the tessellation by 45° .

Note that the unit-cell complex in Fig. 8(a) for the square lattice allows for tessellations [Fig. 8(d)] with nine atoms per unit cell (four of the 11 atoms of \mathcal{C}_{SCU} are shared between pairs of unit cells) such that the number of atoms for an $L \times L$ lattice is of order $9L^2$. The number of Rydberg atoms that can be prepared and controlled in tweezer arrays has recently reached the range of several hundreds [23–25], so that lattices with $\sim 6 \times 6$ sites are already within reach of state-of-the-art platforms.

B. Fibonacci model

The surface code only supports Abelian anyons, which are not sufficient for universal *topological quantum computation*, where gates are implemented fault tolerantly by braiding of localized excitations and measurements correspond to their

fusion [72–74]. The simplest anyon model that supports universal computation by braiding is known as *Fibonacci model* due to the role the Fibonacci numbers play in the fusion rules [75–77]; it may be realized in some fractional quantum Hall states [78,79]. As quasiparticles, the properties of Fibonacci anyons are a consequence of and encoded in the entanglement pattern of the ground state on which they live. The latter turns out to have a representation as a string-net condensate with weights and “string-net” patterns that differ from the surface code [cf. Eq. (38)]. If we consider a Honeycomb lattice with qubits on its edges, the fixed-point ground state of the Fibonacci model has the form [48]

$$|G\rangle = \sum_S \Phi(S) |S\rangle, \tag{44}$$

where the sum goes over all patterns (“string-nets”) S of flipped qubits $|1\rangle$ on the edges of the Honeycomb lattice where *no single string* ends on a vertex. That is, in contrast to the loop patterns \mathcal{C} of the surface code, vertices with *three* fusing strings are allowed. The coefficients $\Phi(S)$ of the superposition are nontrivial functions of the pattern S , so that the condensate is no longer an equal-weight superposition [48,80,81]. It is possible to write down a solvable, local Hamiltonian like Eq. (36) with the exact ground state (44), which is, however, so complicated that it is essentially useless for implementations [48]. This complication, together with the potential usefulness of the model for quantum computation, motivates again the construction of a Rydberg complex \mathcal{C}_{Fib} that implements the tessellated target Hilbert space

$$\mathcal{H}_0[\mathcal{C}_{\text{Fib}}]^{\text{loc}} \simeq \mathcal{H}_T = \text{span} \{ |S\rangle \mid \text{String-net } S \}, \tag{45}$$

which has the dimension $\dim \mathcal{H}_0[\mathcal{C}_{\text{Fib}}] \sim (1 + \varphi^2)^M + (1 + \varphi^{-2})^M$ where M is the number of unit cells of the Honeycomb lattice and $\varphi = (1 + \sqrt{5})/2$ is the golden ratio [82,83]. As for the surface code, $\mathcal{H}_0[\mathcal{C}_{\text{Fib}}]$ is a Hilbert space that cannot be decomposed into factors of local Hilbert spaces.

Since the Honeycomb sites are trivalent, the bit-projector takes now the form

$$u_s \left(\begin{array}{c} \vdots \\ x_{e_1}^1 \\ \vdots \\ x_{e_2}^1 \\ \text{---} \text{---} \text{---} \\ x_{e_3}^1 \\ \vdots \end{array} \right) = (x_{e_1}^1, x_{e_2}^1, x_{e_3}^1) \tag{46}$$

and the check function that specifies the allowed string nets can be written in the compact form

$$f_{\text{Fib}}(x_1, x_2, x_3) = (x_1 \oplus x_2 \equiv x_3) \vee (x_1 \wedge x_2 \wedge x_3) \tag{47}$$

where the first clause $(x_1 \oplus x_2 \equiv x_3)$ realizes the loop constraint (\equiv denotes the *logical equivalence*, which is equivalent to the XNOR-gate as a connective) and the second clause $(x_1 \wedge x_2 \wedge x_3)$ allows for the fusion of three strings. Note that without the second clause we fall back to the loop constraint of the surface code (now on the honeycomb lattice).

Since there are *five* assignments with $f_{\text{Fib}} = 1$, this check function cannot be realized by a single logic gate (despite having three ports) but must be decomposed into a circuit. Furthermore, since the amalgamation of two logic gates always results in a complex with an even number of ports, at least three gates would be necessary to realize the Fibonacci

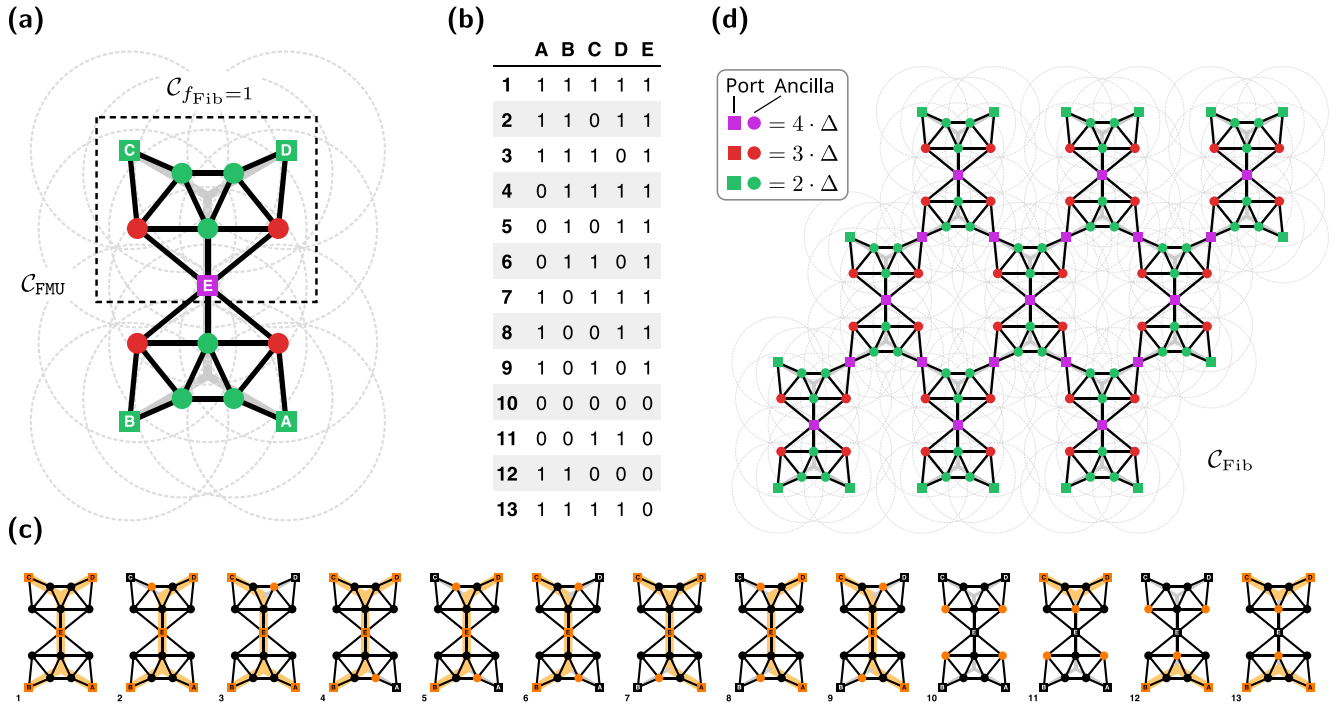


FIG. 9. Fibonacci model. (a) Unit-cell complex C_{FMU} for the Fibonacci model that implements two copies of the single-site check function constraint $f_{\text{Fib}} = 1$ defined in Eq. (47). The complex is the amalgamation of two equivalent eight-atom complexes $C_{f_{\text{Fib}}=1}$ on the two trivalent sites that make up the basis of the honeycomb unit cell. Black edges denote blockades between atoms, gray edges illustrate the underlying Honeycomb lattice. [(b), (c)] Truth table and ground-state manifold of the unit-cell complex. The manifold contains all configurations with closed strings and, in addition, configurations with three strings fusing on a site. This provides the local isomorphism between the string-net Hilbert space \mathcal{H}_T and $\mathcal{H}_0[C_{\text{Fib}}]$. (d) Periodic tessellation C_{Fib} of the complex C_{FMU} . The copies overlap on the edges and are amalgamated at the corresponding ports.

constraint. This already leads into the territory of $\gtrsim 15$ atoms, which we deem too much overhead for a single site. Therefore we follow the same approach as for the logic primitives in Sec. VII: We systematically exclude the existence of complexes $C_{f_{\text{Fib}}=1}$ for $N = 3, 4, \dots, 7$ atoms (Appendix C 2). The approach fails for $N = 8$ and we find the minimal complex in Fig. 9(a) (dashed box). The amalgamation of two of the complexes, one mirrored horizontally, yields the complex C_{FMU} (“Fibonacci model unit cell”) for the two-site unit cell of the Honeycomb lattice, which can then be tessellated as shown in Fig. 9(d). In contrast to the surface code, the detunings are not uniform in this case. The full ground-state manifold of the unit cell is shown in Fig. 9(b). The colored edges in Fig. 9(c) for each ground-state configuration establish the local mapping in Eq. (45). Note how all string-net configurations are allowed except for single strings terminating at a site.

Note that the complex for the hexagonal unit cell with 15 atoms in Fig. 9(a) can be interpreted as the complex on a tilted *square* lattice (by virtually contracting the vertical edges of the honeycomb lattice). This complex, however, is not minimal as we know of a 12-atom complex that realizes the Fibonacci check function constraint on quadrivalent sites.

We conclude this section with a comment on the detunings 4Δ of the ports of the tessellated complex [Fig. 9(d)]. Note that this is the first (and only) complex studied in this paper with detunings exceeding the range $\{1\Delta, 2\Delta, 3\Delta\}$. This seems to be in tension with the claim at the end of Sec. VI (according

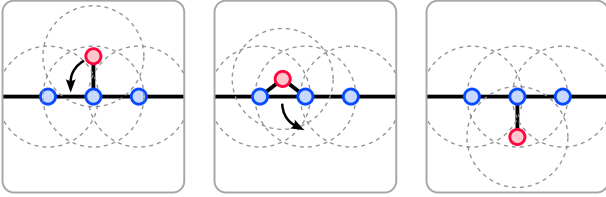
to which this range is sufficient to implement any Boolean constraint). The solution is simple: Instead of amalgamating the single-site complexes $C_{f_{\text{Fib}}=1}$ directly (which yields the 4Δ on the identified ports), one can use a single three-atom LNK-complex to establish the connection between two ports. On each edge of the lattice, a single atom with detuning 4Δ is then replaced by three atoms with detunings 3Δ , 2Δ , and 3Δ , respectively. This modification spoils of course the minimality of the complex, but the corollary in Sec. VI did not come with an assertion for minimality. This observation suggests a tradeoff between minimizing the *number* of atoms and minimizing the *range* of required detunings; a potentially interesting and useful direction for future research (see also Sec. XI).

X. GEOMETRIC OPTIMIZATION

So far we optimized complexes only in terms of their *size* (number of atoms) for a given language. As a result, we ended up with minimal complexes that are defined by their blockade graph B , local detunings $\{\Delta_i\}$, and an assignment of ports ℓ , i.e., atoms that realize the desired language in the ground-state manifold. Remember that in a blockade graph $B = (V, E)$ an edge $e = (i, j) \in E$ between atoms $i, j \in V$ indicates that they are in blockade, i.e., cannot be excited simultaneously. An abstract graph that can be realized in this way by placing atoms in the plane, which are in blockade if and only if their distance

is smaller than some blockade radius r_B is called a *unit disk graph*, and a geometry G_C that realizes a prescribed graph as its blockade graph is a *unit disk embedding* of this graph. So far, the actual geometry G_C of our minimal complexes was only taken into account insofar as a unit disk embedding of the required blockade graph B must *exist*. (Note that there are graphs that cannot be realized as blockade graphs of planar geometries, so that this “geometric realizability” is a nontrivial condition; deciding whether a given graph can be realized in this way is unfortunately NP-hard [84].)

Whenever there exists a planar geometry $G_C = (\mathbf{r}_i)_{i \in V} \in \mathbb{R}^{2N} \equiv \mathfrak{C}_N$ that realizes a prescribed blockade graph, there typically exist many such geometries: In most cases, there is a bit of “wobble room” around a given geometry without changing the blockade graph. In addition, there can be geometrically distinct realizations of the same blockade graph that cannot be continuously deformed into each other without violating the blockade constraints. For example:



This can lead to disconnected regions in the configuration space \mathfrak{C}_N that realize a given blockade graph.

To optimize the geometry of a complex in \mathfrak{C}_N , we have to quantify what we mean by a “good” complex. To this end, we define an *objective function* $\Gamma : \mathfrak{C}_N \rightarrow \mathbb{R}$ that quantifies the quality of the complex and that we seek to minimize. One example is

$$\tilde{\Gamma}(G_C) = \frac{\delta E}{\Delta E} \quad (48)$$

where δE and ΔE are the width of the ground-state manifold and the gap (recall Fig. 2). The problem with Eq. (48) is that its evaluation scales exponentially with the number of atoms N because the computation of δE and ΔE in principle requires access to the complete spectrum of Eq. (1) (which is in general an NP-hard problem [29]). While this is feasible for small complexes, it becomes quickly a bottleneck as $\tilde{\Gamma}$ must be evaluated repeatedly when iteratively optimizing a geometry. Furthermore, in the PXP approximation, interaction energies are either infinite or zero so that $\tilde{\Gamma}$ vanishes whenever the blockade constraints are satisfied. Thus we need a simpler, heuristic quantity that can be directly computed from the geometry of the complex.

A. Geometric robustness

To motivate the quantity we propose as objective function below, we first have to review the role of the blockade radius r_B in the PXP model. In the limit of vanishing driving, the blockade radius r_B is the distance from an atom where the van der Waals interaction matches its detuning: $C_6 r_{B_i}^{-6} \stackrel{!}{=} \Delta_i$. As the detunings can vary from atom to atom in a generic structure \mathcal{C} , so does the blockade radius r_{B_i} (this dependence is quite weak, though). However, as outlined in Sec. III, we

would like to work in the approximate framework of the PXP model with a *unique* blockade radius r_B , because then the effects of interactions between atoms simplify to kinematic constraints encoded in a blockade graph. In the following, we interpret a given blockade graph B as the encoding of the constraints we would like to realize with a structure \mathcal{C} of yet unknown geometry G_C .

We can now introduce two dimensionless quantities. First, the *robustness* of a structure with respect to a given blockade graph $B = (V, E)$ is defined as

$$\xi_B(\mathcal{C}) := \frac{\min_{(i,j) \notin E} d(\mathbf{r}_i, \mathbf{r}_j) - \max_{(i,j) \in E} d(\mathbf{r}_i, \mathbf{r}_j)}{\min_{(i,j) \notin E} d(\mathbf{r}_i, \mathbf{r}_j) + \max_{(i,j) \in E} d(\mathbf{r}_i, \mathbf{r}_j)}, \quad (49)$$

where $d(\mathbf{r}_i, \mathbf{r}_j)$ denotes the Euclidean distance. The robustness is a scale-invariant, finite number $\xi_B(\mathcal{C}) \in [-1, 1]$ where $\xi_B(\mathcal{C}) > 0$ indicates a valid unit disk embedding G_C that realizes the prescribed blockade graph B for blockade radii in some finite interval. Larger positive values of $\xi_B(\mathcal{C})$ indicate more *robust* embeddings with more “wobble room” around the positions without changing the blockade graph, or, equivalently, a wider range of blockade radii that yield the same blockade graph. If $\xi_B(\mathcal{C}) < 0$, the unit disk graph induced by G_C does not match the prescribed blockade graph B .

Similarly, the *spread* of a structure \mathcal{C} is defined as

$$\begin{aligned} s(\mathcal{C}) &:= \frac{\max_i r_{B_i} - \min_i r_{B_i}}{\max_i r_{B_i} + \min_i r_{B_i}} \\ &= \frac{(\max_i \Delta_i)^{1/6} - (\min_i \Delta_i)^{1/6}}{(\max_i \Delta_i)^{1/6} + (\min_i \Delta_i)^{1/6}}. \end{aligned} \quad (50)$$

The spread $s \in [0, 1]$ quantifies the relative variations in blockade radii of a structure (a system with uniform detuning $\Delta_i \equiv \Delta$ has vanishing spread). Just as Eq. (49) does not depend on the length scale, Eq. (50) is independent of the C_6 coefficient, i.e., the strength of the interaction.

We can now take into account the variability of the blockade radius without abandoning the PXP model as follows. We call a structure \mathcal{C} a *valid implementation* of a blockade graph B if

$$s(\mathcal{C}) < \xi_B(\mathcal{C}). \quad (51)$$

This condition ensures that the geometry G_C can be scaled such that all distances of atoms that should (not) be in blockade according to B , are smaller (larger) than the smallest (largest) blockade radius of the structure \mathcal{C} . As this condition is scale invariant, we do not have to specify r_B in the following. Note that all structures presented in this paper are valid in the sense of Eq. (51).

B. Numerical optimization

These considerations suggest the robustness ξ_B as a measure for the quality of geometries. We therefore set $\Gamma = -\xi_B$ to maximize this quantity by minimizing Γ . The blockade graph B and the detunings $\{\Delta_i\}$ are fixed and define the functional properties of the complex; in particular, the spread $s(\mathcal{C})$ is constant. Thus we optimize for geometries that satisfy the validity constraint (51) with a maximal margin between robustness and spread.

We call a complex \mathcal{C} *globally (locally) optimal* if $\xi_B(\mathcal{C}) > 0$ and its geometry is a global (local) minimum of Γ in \mathfrak{C}_N .

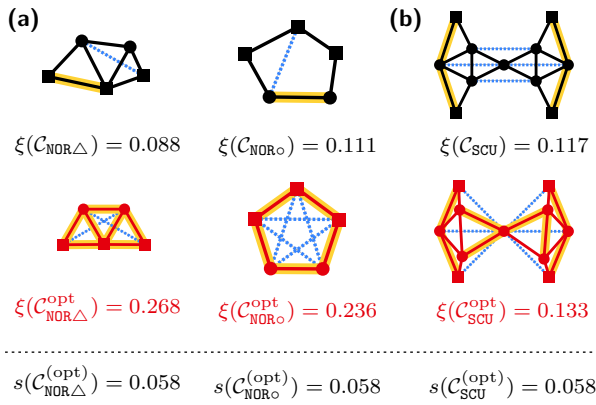


FIG. 10. Optimization (examples). (a) Comparison of perturbed (black) and optimized (red) geometries for the two minimal NOR-complexes. Maximum distance blockades are highlighted yellow, minimum distances of unblocked atoms are indicated by dashed blue edges. The optimal geometries are highly symmetric and match the manually constructed ones in Figs. 6 and 5(c). The robustness for each complex is printed below the geometries and the spread on the bottom of each column (we omit blockade graph indices). Note that $\xi(C_{\text{NOR}\Delta}^{\text{opt}}) > \xi(C_{\text{NOR}\circ}^{\text{opt}})$, which makes the triangular version $\text{NOR}\Delta$ potentially more robust than the ring-shaped $\text{NOR}\circ$. For all geometries the validity constraint $s(C) < \xi(C)$ is satisfied. (b) Comparison of the optimized geometry for the vertex complex C_{SCU} of the surface code (red) and the manually constructed geometry (black) from Fig. 8(a); the robustness increases by $\Delta\xi = 0.016$. Due to unconstrained atoms, the optimization can break the symmetry and produce slightly skewed geometries.

To minimize Γ on the high-dimensional space \mathcal{C}_N , we employ the SciPy implementation [85] of generalized simulated annealing [86,87] in combination with a local optimization based on the Nelder-Mead algorithm [88,89], see Appendix D for details. Remember that the robustness is a scale-invariant quantity, so that the scale of the optimized geometry is arbitrary. For normalization, we rescale the geometries by setting the blockade radius

$$r_B := \frac{1}{2} \left[\max_{(i,j) \in E} d(\mathbf{r}_i, \mathbf{r}_j) + \min_{(i,j) \notin E} d(\mathbf{r}_i, \mathbf{r}_j) \right] \stackrel{!}{=} 1. \quad (52)$$

First, we initialized the algorithm with the hand-crafted geometries of all primitives in Secs. VII and VIII and the vertex complexes in Sec. IX to optimize their robustness (we believe the results to be globally optimal but we did not prove this). With these initial configurations, the optimizer already started with a valid unit disk embedding of B ($\xi_B > 0$) and tried to maximize the robustness further. The results were typically only slightly deformed versions of the manually constructed complexes, confirming our intuition. Some of the primitives [in particular the ring-shaped NOR-complex in Fig. 5(c)] were already optimal due to their high symmetry. In Fig. 10(a) we demonstrate this by comparing slightly perturbed geometries (black) to the subsequently optimized versions (red) for both minimal realizations of the NOR-complex. In particular, we find

$$\xi_{B_{\text{NOR}\Delta}}(C_{\text{NOR}\Delta}^{\text{opt}}) = 0.268 > 0.236 = \xi_{B_{\text{NOR}\circ}}(C_{\text{NOR}\circ}^{\text{opt}}) \quad (53)$$

and conclude that the triangular version $\text{NOR}\Delta$ (Fig. 6) is potentially more robust than the ring-shaped $\text{NOR}\circ$ [Fig. 5(c)]. For both, the validity constraint (51) is safely satisfied ($x \in \{\circ, \Delta\}$),

$$s(C_{\text{NOR}x}^{\text{opt}}) = 0.058 < \xi_{B_{\text{NOR}x}}(C_{\text{NOR}x}^{\text{opt}}). \quad (54)$$

Since the robustness depends only on the maximum (minimum) distance of atoms that are (not) in blockade, there can be atoms with positions that are unconstrained in small regions of the plane. These positions can be chosen by the optimization algorithm at will, leading to slightly skewed geometries that break the natural symmetry of the complex; an example is given by the optimized surface code unit-cell complex in Fig. 10(b). This is an artifact of our particular objective function that can be eliminated by more sophisticated choices for Γ (e.g., motivated by specific experimental requirements). All optimized complexes are accessible online [90], normalized according to Eq. (52).

In a second run, we went one step further and initialized the optimization with geometries that *violated* the prescribed blockade graphs (by placing the atoms randomly). In this case, the algorithm started with $\xi_B < 0$ and first had to identify valid unit disk embeddings by stochastic jumps in the configuration space. These runs typically rediscovered the geometries we already knew. In some cases, alternative geometries were found (which turned out to be local maxima of robustness, though). We conclude that it is not only possible to optimize given geometries but also to *find* them (if they exist), at least for small complexes.

As a final remark, we stress that geometric optimization is in general not *reducible*, i.e., optimizing the primitives of a larger circuit does not necessarily optimize the whole circuit as constraints between primitives are not taken into account by this approach. This is particularly important for tessellated complexes of quantum phases like the spin liquids in Sec. IX, where one should optimize the complete tessellation to minimize unwanted residual interactions that are not present in the optimization of a single-site or unit-cell complex.

XI. OUTLOOK AND COMMENTS

We conclude with a few comments on open questions and directions for future research.

Minimality. To find and prove the minimality of complexes we systematically excluded realizations with fewer atoms. While this approach is more efficient than a brute force search (by exploiting constraints from the language, the detunings, and the planar geometry), it is still far from trivial and cannot be easily automated. It would be both interesting and useful to develop an algorithm that given a uniform language, constructs a *minimal* graph with weighted nodes, and a labeled node for each letter position of the language, such that each *maximum-weight independent set* [91] is in one-to-one correspondence with a word of the language. We are neither aware of such an algorithm nor of statements on the complexity to find minimal solutions. (Note that a solution of this problem might not even be a unit disk graph, i.e., realizable by the blockade graph of a planar Rydberg complex.)

Optimization. It is clear that our treatment of optimization in Sec. X only scratches the surface. First, our choice

of the objective function Γ is heuristic and other functions may be more appropriate for specific experimental settings. This would change the “optimal” geometries of complexes, of course. Second, there is a plethora of alternative numerical algorithms available that could be used to minimize the objective function more efficiently. In particular the existence of distinct geometries that are separated by complexes that violate the blockade graph may require more sophisticated algorithms to escape locally optimal configurations and find the global optimum. The algorithms also should scale well with the size of the complex because, as mentioned previously, tessellations should be optimized as a whole to take into account constraints between its primitives.

If we go one step further and ask for an algorithm that *constructs* geometries from a given blockade graph, we quickly enter complexity hell: Deciding whether a given blockade graph can be realized as a unit disk graph is known to be NP-hard [84]. Even if we are *promised* to be given a unit disk graph as blockade graph, there is *no* efficient algorithm that outputs the geometry of a complex that realizes it. This is so because there are unit disk graphs that require exponentially many bits to specify the positions of the nodes [92]. To add insult to injury, even finding certain *approximations* of unit disk graph embeddings are known to be NP-hard [93]. None of these statements prevent us from looking for heuristic algorithms to solve these problems for specific cases, of course (as we demonstrated in Sec. X).

Uniformity. Most of the complexes discussed in this paper make use of atom-specific detunings [e.g., Figs. 6 and 9(d)]. Only the surface code tessellation in Fig. 8(d) is uniform in detunings, at least in the bulk. While it is possible to realize atom-specific detunings [54,55], single-site addressability adds significant experimental overhead. Thus it is reasonable to ask whether complexes with nonuniform detunings can be replaced by (potentially larger) complexes with uniform detunings (without adding additional degrees of freedom). For instance, there is a third minimal NOR-complex with uniform detuning $\Delta_i \equiv \Delta$. However, in amalgamated circuits this uniformity is often destroyed—on the contrary, it is the *nonuniformity* of the XNOR-complex (Fig. 6) that made the bulk of the surface code uniform [Fig. 8(d)]. The quest for uniformity is therefore best formulated on the level of complete circuits or tessellations.

Beyond planarity. We focused completely on *planar* Rydberg complexes to comply with the restrictions of current experimental platforms: For the addressability of single atoms it is simply convenient to have a dimension of unimpeded access. However, technologically, three-dimensional structures of Rydberg atoms are possible and have been experimentally demonstrated [5,38]. Releasing the planarity constraint drastically changes the rules for the construction of Rydberg complexes. For instance, ports that are located *inside* a 2D complex (and would require expensive crossings to be routed to the perimeter) can be directly accessed from the third dimension, possibly simplifying certain functional primitives. Note, however, that at least the logic primitives in Fig. 6 do *not* profit from a third dimension. (This follows from the proofs in Appendix A.)

Beyond the PXP approximation. Our construction of Rydberg complexes was based on the assumption that atoms

within the blockade radius can never be simultaneously excited, while atoms separated by more than the blockade radius do not interact at all; this “PXP approximation” implements the dynamical effect of the interactions as a kinematic constraint. In reality, however, the atoms interact via the van der Waals interaction $U_{\text{vdW}} = C_6 r^{-6}$, which contributes also beyond the blockade radius, can lift the degeneracy δE of the ground-state manifold, and reduce the gap ΔE that separates it from excited states. One therefore expects that complexes with $\delta E \approx 0$ in the vdW model are geometrically more constrained than in the PXP model. This has an effect on the geometrical optimization of complexes (see above) and the appropriate choice of the objective function: To take into account residual interactions properly, heuristic functions like the robustness should be replaced by realistic functions like Eq. (48), at least for small complexes where they can be computed exactly.

We checked that the three primitives in Fig. 5 can be realized with perfect degeneracy $\delta E = 0$ and gap $\Delta E > 0$ in the vdW model by small adjustments of the detunings to balance residual interactions. In principle, a NOR-complex can even be realized with only three atoms, arranged in a triangle with precisely defined shape. This is possible, because the two ancillas in Fig. 5(c) were only necessary to balance the energies of states with one and two input ports active; in the vdW model, the same can be achieved by exploiting the residual interaction between the two input ports. Which version of the NOR-complex is more useful for implementations is an open question.

Quantum phase diagrams. In this paper, we only studied the ground-state manifold of the Hamiltonian (1) without quantum fluctuations ($\Omega_i = 0$). As has been demonstrated in Refs. [41,42], the interplay of quantum fluctuations ($\Omega_i > 0$) and the strong blockade interactions can give rise to interesting many-body quantum phases at zero temperature. Thus it seems natural to explore the quantum phase diagrams of the proposed spin liquid tessellations in Sec. IX, for example numerically using density matrix renormalization group (DMRG) techniques. Analytically, one could derive the effective Hamiltonians on the constructed low-energy manifolds for finite but small Rabi frequencies $\Omega_i \ll \Delta E$ in perturbation theory [94]. Note that in general one expects the relative strengths of the effective terms to depend on the specific complex used to implement the local constraints. This raises the subsequent question whether these couplings can be *tuned* by modifications of the used complexes.

Dynamical preparation. In recent experiments [44], dynamical preparation schemes have been used to prepare long-range entangled many-body states out-of-equilibrium [45,46]. The idea is to use “quasiadiabatic” protocols $\Omega_i(t)$ and $\Delta_i(t)$ where the detuning increases continuously to its target value while a finite Rabi frequency ensures the coupling of different excitation patterns. This allows for the preparation of nontrivial superpositions of states in the low-energy subspace of the classical Hamiltonian (1). It would be interesting to explore the states of the proposed tessellations that can be prepared by such dynamical protocols numerically, and study the effects of defects in the intended logic of the complexes due to local excitations. Similar questions arise for the primitives in Secs. VII and VIII and circuits built from these by amalgamation.

Alternative platforms. Rydberg atoms in optical tweezer arrays are the most prominent and advanced platform with a high level of coherent control that features a blockade mechanism. Our paper originated in this context and is therefore phrased in its terminology. It is important to keep in mind, however, that our main results only require some sort of blockade mechanism, fine-grained control over the geometric structure of the system, and locally tunable energy shifts (like chemical potentials or magnetic fields). A natural follow-up question is then whether there are alternative physical systems with these features. Both our abstract framework and the introduced complexes could be applied to and realized by such systems.

XII. SUMMARY

In this paper, we developed a framework to design planar structures of atoms, which can be excited into Rydberg states under the constraint of the Rydberg blockade mechanism (“Rydberg complexes”). Our framework targets the preparation of degenerate ground-state manifolds that are characterized locally by arbitrary Boolean constraints. We proved that the truth table of an arbitrary Boolean function can be realized as ground-state manifold by decomposing its circuit representation into three primitives that leverage the Rydberg blockade. Motivated by this existence claim, we then presented provably minimal complexes that realize the most important primitives of Boolean circuits, including a crossing complex that is needed to embed nonplanar circuits into the plane. As an application of our framework, we constructed periodic Rydberg complexes with degenerate ground-state manifolds that map locally on the nonfactorizable string-net Hilbert spaces of the surface code (with Abelian topological order) and the Fibonacci model (with non-Abelian topological order). In combination with quantum fluctuations, these structures may be the starting point to prepare topologically ordered states in upcoming quantum simulators. We concluded the paper with a discussion of the geometric optimization of Rydberg complexes using numerical algorithms to increase their robustness against geometric imperfections and the effects of long-range van der Waals interactions.

Our results highlight the versatility of planar structures of atoms that interact via the Rydberg blockade mechanism. We provide a conceptual foundation for the rationales of *geometric programming*, the encoding and solution of problems by tailoring the geometry of atomic systems, and *synthetic quantum matter*, the goal-driven design of quantum materials on the atomic level. Due to the noisiness of near-term experimental platforms, the latter seems particularly promising because quantum phases come with an inherent robustness against a finite density of excitations. This robustness is less clear in the geometric programming paradigm where the search for (near-)optimal solutions can be severely impeded by defects in the prepared states, especially at scale.

Note added. We became aware of related results [33,34]; the authors of both publications focus on optimization problems and find some of the primitives discussed in this paper. (The ring-shaped NOR-gate and the crossing is found by Nguyen *et al.* [33] and the triangle shaped XNOR-gate by Lanthaler *et al.* [34].) Both papers follow the rationale of

geometric programming, so that their motivation, approach and framework differ from ours.

ACKNOWLEDGMENTS

We thank Sebastian Weber for comments on the manuscript. This project has received funding from the French-German collaboration for joint projects in Natural, Life and Engineering (NLE) Sciences funded by the Deutsche Forschungsgemeinschaft (DFG) and the Agence National de la Recherche (ANR, project RYBOTIN).

APPENDIX A: MINIMALITY OF LOGIC PRIMITIVES

Here we prove the claims in Secs. VI and VII about the minimality of the logic primitives. The proofs in this section do *not* require geometric arguments (i.e., whether a given blockade graph is a unit disk graph or not). This makes the claims independent of the embedding dimension; in particular, they remain valid for three-dimensional complexes.

We start with a few general remarks. First, the languages we seek to implement as ground-state manifolds (GSM) are *irreducible* in the sense that they cannot be written as a product of two smaller languages. (The product of two formal languages is simply the set of all words from the first concatenated with all words from the second.) This is easy to check for all Boolean gates by inspecting their truth tables. The crucial point is that irreducible languages can only be implemented by complexes with *connected* blockade graphs.

Second, because we are only interested in GSM of PXP models, all detunings can be assumed to be strictly positive, $\Delta_i > 0$. Indeed, atoms with *negative* detuning cannot be excited in the GSM so that they can be deleted from the complex without changing the GSM (and without closing the gap). The argument against atoms with *vanishing* detuning is more subtle. If such an atom is not excited in any of the GSM states, it can be deleted without changing the GSM. If it *is* excited in some of the GSM states, there is always an otherwise identical state in the GSM where it is not excited. Such an atom therefore must be a port because as an ancilla it would add internal degrees of freedom that are not accessible via the ports (this follows from our definition of a complex). The language that corresponds to a complex with a zero-detuning port therefore has the property that for every word with a “1” at the corresponding position, there must be an otherwise identical word with a “0”. (This does not imply that the language is reducible; for example, $L = \{111, 011, 000\}$ has this property for the first letter but is irreducible.) While such languages do exist, they cannot be truth tables of Boolean functions because such a port cannot be used as an input or an output (assuming we forbid “dummy” inputs that have no effect on the output). All languages discussed and implemented in this paper (also the ones for the vertex complexes of spin liquids) do *not* have this property, hence we can assume nonvanishing detunings.

Because of the positivity of all detunings, ground states are always given by *maximal independent sets* (MIS*) of the blockade graph. [A *maximal independent set* is a subset of vertices such that (1) no two vertices of the set are connected by an edge of the graph and (2) no vertex can be added to the set without violating (1). *Maximum independent sets*

(MIS) are the largest *maximal* independent sets.] The inverse is not necessarily true: Depending on the detunings, not every MIS* describes a ground-state configuration (an example is the ring-like NOR-complex).

1. CPY-complex

Lemma 1. A CPY-complex cannot be realized with less than four atoms (one ancilla).

Proof. Assume there is a complex without ancillas described by

$$H = -\Delta_1 n_1 - \Delta_2 n_2 - \Delta_3 n_3 =: E_{n_1 n_2 n_3}. \quad (\text{A1})$$

Since $(n_1 n_2 n_3) = (111)$ must be a ground state of the complex, none of the pairs of the atoms can be in blockade so that there is no kinematic constraint on the configurations $(n_1 n_2 n_3)$. To be a CPY-complex, it must be

$$-(\Delta_1 + \Delta_2 + \Delta_3) = E_{111} \stackrel{!}{=} E_{000} = 0 \quad \text{and} \quad E_{n_1 n_2 n_3} > 0$$

for all $(n_1 n_2 n_3) \neq (000), (111)$. (A2)

The finite-gap condition requires in particular $\Delta_i > 0$ for all $i = 1, 2, 3$, which leads to $-(\Delta_1 + \Delta_2 + \Delta_3) < 0$ and thereby contradicts the degeneracy condition.

Alternative argument. The copy language $L_{\text{CPY}} = \{000, 111\}$ is irreducible. Since (111) must be in the GSM, the only admissible blockade graph is the trivial graph on three vertices without edges: $B = (V = \{1, 2, 3\}, E = \emptyset)$. But a disconnected blockade graph cannot implement an irreducible language. ■

2. NOR-complex

Lemma 2. A NOR-complex cannot be realized with less than five atoms (two ancillas).

Proof. We show that a NOR-complex cannot be realized with one ancilla or less. First, assume there is no ancilla so that the Hamiltonian is again

$$H = -\Delta_1 n_1 - \Delta_2 n_2 - \Delta_3 n_3 =: E_{n_1 n_2 n_3}, \quad (\text{A3})$$

now with potential kinematic constraints due to the Rydberg blockade. The conditions for a NOR-complex demand the equality of the following energies:

$$E_{001} = -\Delta_3, \quad (\text{A4a})$$

$$E_{010} = -\Delta_2, \quad (\text{A4b})$$

$$E_{100} = -\Delta_1, \quad (\text{A4c})$$

$$E_{110} = -\Delta_1 - \Delta_2. \quad (\text{A4d})$$

It follows immediately $\Delta_1 = \Delta_2 = \Delta_3$ and $\Delta_1 = 0$ so that all detunings must vanish. But then $(n_1 n_2 n_3) = (000)$ is— independent of the configuration and its implied kinematic constraints—degenerate with the four states that belong to the NOR-manifold (which it must not be).

Alternative argument. The NOR-language $L_{\text{NOR}} = \{001, 010, 100, 110\}$ is irreducible and forbids a blockade between the two input ports [because of (110)]. The only consistent blockade graph B is therefore the line graph of three vertices. But this graph has only *two* maximal independent sets, whereas we need at least *four* to realize L_{NOR} .

So let us assume a system with one additional ancilla,

$$H = -\Delta_1 n_1 - \Delta_2 n_2 - \Delta_3 n_3 - \Delta_4 \tilde{n}_4, \quad (\text{A5})$$

and an arbitrary geometry that may lead to kinematic constraints on the allowed configurations. Let now $\varepsilon(n_1 n_2 n_3)$ denote the *minimal* energy of the system *without* the contribution from the ports under the “boundary condition” that these are in the state $(n_1 n_2 n_3)$ and under the kinematic constraints imposed by the Rydberg blockade; furthermore, set $E_{n_1 n_2 n_3} := -\Delta_1 n_1 - \Delta_2 n_2 - \Delta_3 n_3 + \varepsilon(n_1 n_2 n_3)$. In the current situation with only one ancilla, it is either $\varepsilon(n_1 n_2 n_3) = 0$ if the minimum is obtained by $\tilde{n}_4 = 0$, or $\varepsilon(n_1 n_2 n_3) = -\Delta_4$ if $\tilde{n}_4 = 1$ minimizes the energy [and this is consistent with the configuration $(n_1 n_2 n_3)$]. With this notation, the conditions to be a NOR-complex take the following form. First, the degeneracy of the NOR-manifold demands the equivalence of the following expressions:

$$E_{001} = -\Delta_3 + \varepsilon(001), \quad (\text{A6a})$$

$$E_{010} = -\Delta_2 + \varepsilon(010), \quad (\text{A6b})$$

$$E_{100} = -\Delta_1 + \varepsilon(100), \quad (\text{A6c})$$

$$E_{110} = -\Delta_1 - \Delta_2 + \varepsilon(110), \quad (\text{A6d})$$

which immediately implies

$$\Delta_1 = \varepsilon(110) - \varepsilon(010), \quad (\text{A7a})$$

$$\Delta_2 = \varepsilon(110) - \varepsilon(100), \quad (\text{A7b})$$

$$\Delta_3 = \varepsilon(110) + \varepsilon(001) - \varepsilon(100) - \varepsilon(010). \quad (\text{A7c})$$

Second, the gap condition requires (among other conditions)

$$\varepsilon(000) = E_{000} \stackrel{!}{>} E_{100} = -\Delta_1 + \varepsilon(100) = \varepsilon(010) - \varepsilon(110) + \varepsilon(100) \quad (\text{A8a})$$

$$\Leftrightarrow \varepsilon(000) + \varepsilon(110) > \varepsilon(010) + \varepsilon(100) \quad (\text{A8b})$$

because a state with $(n_1 n_2 n_3) = (000)$ is not allowed in the NOR-manifold. Note that the only kinematic constraints on the ancilla in Eq. (A8b) can come from the two input vertices since $n_3 = 0$ for all four terms. We show now that Eq. (A8b) cannot be satisfied with a single ancilla.

Consider first the case where $\Delta_4 \leq 0$. Then the minimal energy under any condition $(n_1 n_2 n_3)$ is reached by switching the ancilla *off*, $\tilde{n}_4 = 0$ (this is possible for all kinematic constraints), so that $0 + 0 > 0 + 0$ leads to a contradiction. Thus we have to assume $\Delta_4 > 0$ (this we could have anticipated from the arguments above). Now the energy can be lowered by switching the ancilla *on*, but this might be forbidden by the kinematic constraints for certain boundary conditions $(n_1 n_2 n_3)$. We consider three cases:

(1) No blockade between the two inputs and the ancilla. In this case, the ancilla will be switched on in all four terms of Eq. (A8b) so that $-\Delta_4 - \Delta_4 > -\Delta_4 - \Delta_4$ violates the gap condition.

(2) The ancilla is in blockade with one of the inputs. W.l.o.g. let n_1 be in blockade with \tilde{n}_4 . Then Eq. (A8b) reads $-\Delta_4 + 0 > -\Delta_4 + 0$ which again violates the gap condition.

(3) The ancilla is in blockade with both inputs. Now Eq. (A8b) reads $-\Delta_4 + 0 > 0 + 0$ which is in contradiction with the assumption $\Delta_4 > 0$.



FIG. 11. The line graph is the only connected blockade graph on five vertices with (at least) four maximal independent sets (orange vertices), (at least) one of which has (at least) three vertices. To realize the state (111), the vertices $\{1, 3, 5\}$ must be chosen as ports, with 3 as output; the four maximal independent sets then realize the truth table of AND (these four states cannot be made degenerate while maintaining a gap, see text).

In conclusion, we showed that it is impossible to satisfy the gap condition with a single ancilla.

Alternative argument. Of the six connected graphs on four vertices, only the “tetrahedron graph” has four maximal independent sets (the others have at most three), which is necessary to realize the four words in L_{NOR} . But none of these four maximal independent sets contain more than one vertex [which would be necessary for (110)]. ■

3. AND-complex, OR-complex and XNOR-complex

Lemma 3. AND-, OR- and XNOR-complexes cannot be realized with less than six atoms (three ancillas).

Proof. All these complexes contain the state (111) such that no two ports can be in blockade with each other. This implies that no realization of these gates is possible with four or less atoms as the only connected blockade graph, which fulfills this constraint is the star graph of the CPY-complex (which has only two MIS*).

The number of vertices is still small enough to systematically screen the 21 connected graphs on five vertices and select the 11 relevant ones with at least four maximal independent sets. One can check that only the chain graph has a MIS* with (at least) three vertices, which is needed to realize the port configuration (111) (Fig. 11). This MIS* contains the vertices $\{1, 3, 5\}$ of the chain, which we therefore must choose as ports: $(n_1 n_3 n_5) = (111)$. With these ports, the set of four MIS* then realizes the language $L = \{111, 100, 001, 000\}$, which we identify as the truth table of the AND-gate if we choose the port on the central atom 3 as output. This proves that the OR- and XNOR-complex cannot be realized with five atoms (even if another port is declared as output).

So far the arguments were purely *kinematic* insofar as only the blockade constraints and the knowledge that the GSM is generate by maximal independent sets were used. To exclude the AND-gate, this is not enough, and we have to use *energetic* arguments by studying possible choices for detunings. The degeneracy of the GSM requires the following four expressions to be equal,

$$E_{111} = -\Delta_1 - \Delta_3 - \Delta_5, \quad (\text{A9a})$$

$$E_{100} = -\Delta_1 - \Delta_4, \quad (\text{A9b})$$

$$E_{001} = -\Delta_2 - \Delta_5, \quad (\text{A9c})$$

$$E_{000} = -\Delta_2 - \Delta_4, \quad (\text{A9d})$$

which immediately implies $\Delta_4 = \Delta_5$ and therefore $\Delta_3 = 0$, which is not allowed (remember that vanishing detunings are forbidden). This proves that also the AND-complex cannot be realized with five atoms. ■

4. NAND-complex and XOR-complex

Lemma 4. NAND- and XOR-complexes cannot be realized with less than seven atoms (four ancillas).

Proof. The truth tables of both NAND and XOR contain the states (110), (101), and (011) so that no two ports can be in blockade with each other. This excludes a realization with less than four atoms (see Appendix A 3). If two ancillas are available, we can switch one of the input ports on; this switches (at least) one ancilla off. The remaining two ports and (at most) one ancilla then must realize the NOT-language $L_{\neg} = \{01, 10\}$. This is impossible since the two ports cannot be directly connected and the only blockade graph with a single ancilla realizes the LNK-language $L_{\text{LNK}} = \{00, 11\}$. So let us assume that the complexes can be realized with three ports and three ancillas. For the following arguments, only the edges between ports and ancillas are of importance; potential blockades between ancillas can be ignored. We consider three cases:

(1) There is at least one port that connects to all three ancillas. If this port is on, all ancillas are off, hence the two remaining ports must be on as well; but then at least two of the three states (110), (101), and (011) cannot be realized in the GSM.

(2) There is at least one port that connects to a single ancilla. This edge can be interpreted as an amalgamated NOT-complex. If we delete the port, subtract its detuning from the connected ancilla, and declare the latter as a new port, the new complex of five atoms realizes the truth table of the original complex with one column inverted (w.l.o.g. the first one). For both gates, this new manifold contains the states (010), (001), and (111) (plus another one that depends on the gate). The only blockade graph on five vertices with at least four MIS*, one of which contains at least three vertices [needed for (111)], has been identified in Appendix A 3 as the line graph. There it has also been shown that there is no assignment of detunings that realizes a fourfold degenerate GSM.

(3) All inputs are connected with exactly two ancillas. There are three possibilities to connect three ports with two ancillas each (Fig. 12). By inspection one shows that in all three cases there is a pair of ports that, when activated, forces all ancillas connected to the third port to be off; as this forces the third port to be on, at least one of the states (110), (101), and (011) cannot be realized in the GSM.

This proves that the NAND- and XOR-complex cannot be realized with six atoms. ■

Note. Removing a NOT-complex by deleting the port, subtracting its detuning from its ancilla, and declaring the ancilla as new port, is the inverse of amalgamation; let us call it *amputation*. One has to make sure that the subtraction of the detuning of the port Δ_p from the detuning of its adjacent ancilla Δ_a does not lead to negative (or vanishing) detunings

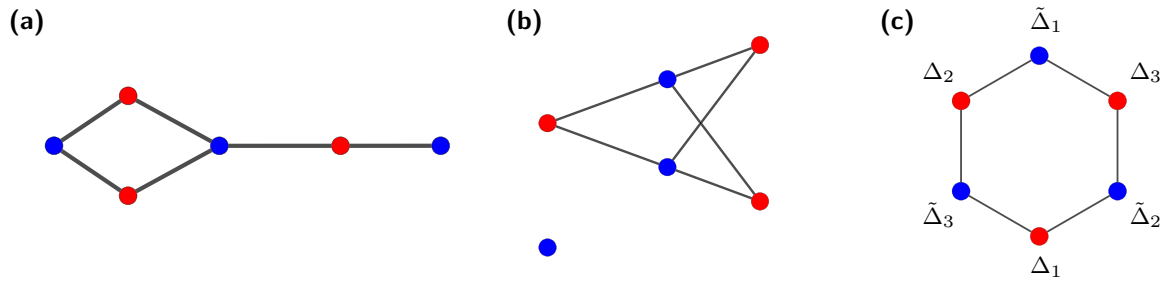


FIG. 12. The three bipartite graphs between three ports (red) and three ancillas (blue) where all ports have degree two. Note that these do not represent complete blockade graphs as we omit blockades between ancillas. The detunings in (c) are used in Appendix A 5.

on the ancilla (= new port). Indeed, if $\Delta_p > \Delta_a$, the port would be always on in all ground-state configurations; this makes the port superfluous and the language of the GSM reducible. If $\Delta_p = \Delta_a$, the language of the original complex would have the property that for every word with a “0” at the corresponding position, there is a otherwise identical word with a “1”. This is the dual property of the one discussed at the beginning of Appendix A and no language discussed in this paper has this property.

5. Uniqueness of the blockade graph of the minimal XNOR-complex

In contrast to the minimal NOR-complexes (for which there are different blockade graph realizations), there is only one realization of the minimal XNOR-complex. This will be useful in Appendix C 2 to prove the minimality of the vertex complex of the Fibonacci model.

Lemma 5. The blockade graph of the minimal XNOR-complex with six atoms (Fig. 6) is unique.

Proof. We showed in Appendix A 3 that a XNOR-complex needs at least six atoms; so let us assume we have six atoms at our disposal. We now try to contrive a complex that realizes the language $L_{\odot} = \{001, 010, 100, 111\}$ systematically:

(1) Assume there exists such a complex with at least one port that connect to only one ancilla. If this port is amputated, the remaining five atoms realize the XOR-language $\bar{L}_{\odot} = \{101, 110, 000, 011\}$, which is impossible as shown in Appendix A 4.

(2) Assume at least one port connects to all three ancillas. If this port is switched on, all ancillas are switched off and therefore the other two ports must be active. This is inconsistent with one of the states (001), (010), and (100).

(3) Because of (1) and (2), only the case where all ports connect to two ancillas remains. There are three classes of blockade graphs that satisfy this, Fig. 12. The first two graphs in Fig. 12 can be immediately excluded as they are inconsistent with the states (001), (010), and (100) (= only one port activated). Only the “hexagon graph” in Fig. 12 remains as a possible blockade structure between ports and ancillas. Without additional blockades between the ancillas, the maximal independent sets of this graph allow for the states $\{000, 001, 010, 100, 111\} \supset L_{\odot}$.

Let $\Delta_{1,2,3}$ denote the detunings of the three ports and $\tilde{\Delta}_{1,2,3}$ the detunings of the three ancillas (where $\tilde{\Delta}_i$ describes the ancilla opposite of port i , Fig. 12). In the state (100), only the first port is excited. So the opposite ancilla must be excited

as well to block the two other ports (if this ancilla were off, one could lower the energy by switching the other two ports on). To balance this state energetically with the state (111), the detuning of the ancilla must equal the sum of the detunings of its two adjacent ports. Due to the permutation symmetry of L_{\odot} and the rotation symmetry of the “hexagon graph”, this argument is valid for all three ancillas,

$$\tilde{\Delta}_1 = \Delta_2 + \Delta_3, \quad \tilde{\Delta}_2 = \Delta_1 + \Delta_3, \quad \text{and} \quad \tilde{\Delta}_3 = \Delta_1 + \Delta_2. \quad (\text{A10})$$

Because all detunings must be positive, this implies for any pair of ancillas

$$-\tilde{\Delta}_i - \tilde{\Delta}_j < -\Delta_1 - \Delta_2 - \Delta_3 = E_{111}. \quad (\text{A11})$$

Since (111) must be in the GSM (i.e., E_{111} must be the lowest allowed energy), there must be an additional blockade between all pairs of ancillas to prevent them from being excited simultaneously. This yields the blockade graph of the XNOR-complex depicted in Fig. 6. It has only four maximal independent sets that realize the language $L_{\odot} = \{001, 010, 100, 111\}$. The choices of the port detunings $\Delta_i > 0$ are arbitrary; the ancilla detunings are then given by Eq. (A10).

We conclude that the blockade graph of the minimal realization of a XNOR-complex with six atoms is unique (there is only freedom in choosing the detunings). In addition, we proved that no *strict superset* of L_{\odot} can be realized by a complex with six atoms or less (this is used in Appendix C 2). ■

APPENDIX B: CONSTRUCTING SUBCOMPLEXES

Here we discuss a method to construct subcomplexes by fixing a port in the active state and deleting its adjacent ancillas in the blockade graph. This method is used in the proofs of Appendix C and the final remark of Sec. VI. Consider a complex \mathcal{C} that realizes a language L with ports that are not in blockade with each other. We can select one of the ports p and define the sublanguage $L_p \subset L$ of words $x \in L$ with $x_p = 1$. Our goal is to construct a L_p -complex \mathcal{C}'_p where L'_p is obtained from L_p by deleting the constant letter at position p that corresponds to the fixed port. The simplest solution is to keep the geometry of the complex \mathcal{C} and increase the detuning of the fixed port Δ_p , thereby creating a gap between states of the original GSM where the port is on and states where it is off; the port can then be downgraded to an ancilla. In all states of the new GSM this ancilla is active, while its adjacent ancillas are inactive. This suggests that one can delete these

atoms to obtain a smaller complex C'_p that realizes the same language L'_p :

Lemma 6. Let the finite complex C realize the irreducible language L with ports that are not in blockade with each other (with $\delta E = 0$ and $\Delta E > 0$). Consider one of the ports p with detuning $\Delta_p > 0$ and let the languages L_p and L'_p be defined as above. Then the structure C'_p obtained from C by deleting the port p and all its adjacent ancillas is a L'_p -complex if the ports of C'_p are inherited from C in the natural way.

Proof. First, note that since L is irreducible, it is $L_p \neq \emptyset$, i.e., there are configurations in the GSM of C where the port p is active. We have to show two things: (a) the structure C'_p together with the inherited ports is a complex (i.e., its ground states can be labeled by the configurations of the ports), and (b) the language that describes this GSM is L'_p .

Let the GSM of the new structure C'_p be defined by $\delta E = 0$ (since the structure is finite, it is automatically $\Delta E > 0$). Every kinetically allowed (= admissible) configuration in this GSM can be *extended* to an admissible configuration of C by setting the deleted ancillas to *off* and the port p to *on*. If $E_0(C'_p)$ denotes the ground-state energy of C'_p and $E_0(C)$ the same for C , this implies that $E_0(C) \leq E_0(C'_p) - \Delta_p$. Conversely, because $L_p \neq \emptyset$, there are admissible configurations in the GSM of C where the port p is *on* and, consequently, all adjacent ancillas are *off*. By *truncating* the configurations of the adjacent ancillas and the port p , this yields a admissible configuration for C'_p with energy $E_0(C) + \Delta_p$ so that $E_0(C'_p) \leq E_0(C) + \Delta_p$. In combination, we have

$$E_0(C'_p) = E_0(C) + \Delta_p \quad (\text{B1})$$

for the ground-state energy of the new structure C'_p . Using this result and the mappings of *extension* and *truncation*, we can draw two conclusions:

(1) Every configuration in the GSM of C'_p can be *extended* to a configuration in the GSM of C , which corresponds to a word in L_p . We can immediately conclude two things:

(i) Since the extended configurations must be distinguishable by the ports of the *complex* C ignoring port p (this port is always *on* for configurations in L_p), and because these ports are inherited by the structure C'_p , we can conclude that the configurations of the GSM of C'_p can also be distinguished by these ports. This makes C'_p a *complex* that realizes some language $L^?$.

(ii) Every word in $L^?$ is mapped by the extension to a word in L_p , which implies $L^? \subseteq L'_p$.

(2) Conversely, every configuration in the GSM of C , which corresponds to a word in L_p can be *truncated* to an admissible configuration of C'_p with energy $E_0(C) + \Delta_p = E_0(C'_p)$, which implies $L'_p \subseteq L^?$.

In conclusion, we showed that $L^? = L'_p$ and therefore that C'_p is indeed a L'_p -complex. ■

APPENDIX C: MINIMALITY OF SPIN LIQUID PRIMITIVES

1. Vertex/Unit cell complex for the surface code (C_{SCU})

Lemma 7. The vertex complex (unit-cell complex) C_{SCU} of the surface code on the square lattice cannot be realized with less than 11 atoms.

Proof. Here we show that the vertex complex of the surface code on the square lattice requires at least 11 atoms; to this end, we use and expand on the tricks introduced in Appendix A 4. First, note that the GSM is symmetric under the permutation of ports [Fig. 8(b)] and includes the state (1111), i.e., no two ports can be in blockade with each other. In addition, the GSM is symmetric under the simultaneous inversion of an even number of letters in all words (= columns),

$$L_{\text{SCU}} \equiv \begin{pmatrix} 1111 \\ 1100 \\ 0011 \\ 1001 \\ 0110 \\ 0101 \\ 1010 \\ 0000 \end{pmatrix} \xrightarrow{\text{inv. 4. letter}} \bar{L}_{\text{SCU}} \equiv \begin{pmatrix} 1110 \\ 1101 \\ 0010 \\ 1000 \\ 0111 \\ 0100 \\ 1011 \\ 0001 \end{pmatrix} \xrightarrow{\text{inv. 3. letter}} L_{\text{SCU}} = \begin{pmatrix} 1100 \\ 1111 \\ 0000 \\ 1010 \\ 0101 \\ 0110 \\ 1001 \\ 0011 \end{pmatrix} \xrightarrow{\text{inv. 2. letter}} \bar{L}_{\text{SCU}} = \begin{pmatrix} 1000 \\ 1011 \\ 0100 \\ 1110 \\ 0001 \\ 0010 \\ 1101 \\ 0111 \end{pmatrix} \dots \quad (\text{C1})$$

Let us now systematically exclude the existence of surface code complexes with $N \leq 10$ atoms:

(1) $N = 8$: If one fixes one port of a surface code complex as active, the remaining three ports realize a XNOR-complex with at least two atoms less than the surface code complex (because the active port deactivates at least one ancilla permanently). Since we proved in Appendix A 3 that XNOR-complexes require at least six atoms, this implies immediately that the surface code complex cannot be realized with $N < 8$ atoms.

(2) $N = 8$: If there are at least two ports that are connected to only one ancilla each, we can consider these as amalgamated NOT-complexes and amputate two of them (see

the note in Appendix A 4), thereby creating a complex with only six atoms that realizes the same GSM due to the inversion symmetry detailed in Eq. (C1). Since this is not possible, there can be at most one port that connects to only one ancilla. Choose one of the other ports that connect to at least two ancillas and again fix it in the active state (here we use the permutation symmetry of L_{SCU}). This produces a complex with at most five atoms (the fixed port plus at least two ancillas are removed from the surface code complex) that realizes again the XNOR-manifold, which is impossible. Hence the surface code complex cannot be realized with eight atoms.

(3) $N = 9$: To show that the complex cannot be realized with nine atoms we consider three cases:

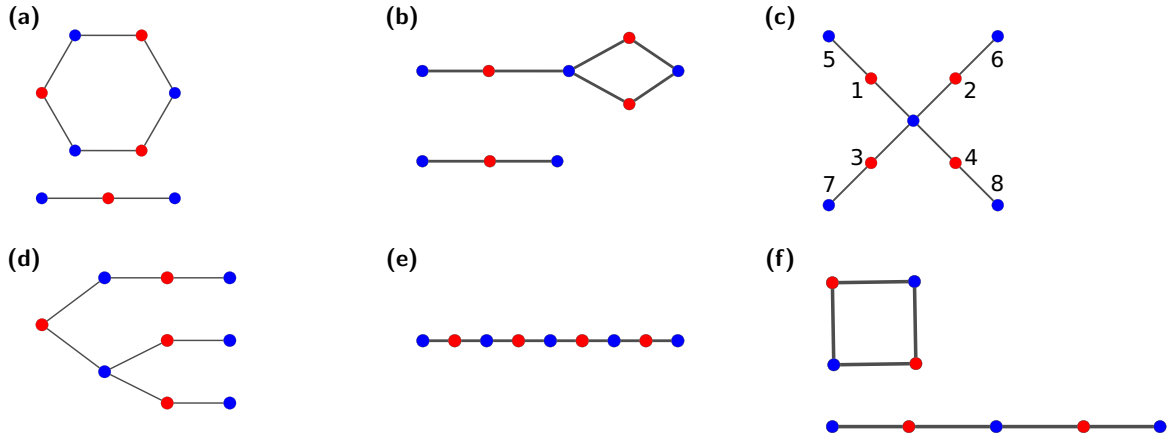


FIG. 13. The remaining six classes of blockade graphs for the surface code vertex complex on nine atoms with ports of degree 2 and without disconnected ancillas. Ports (ancillas) are colored red (blue) and connections between ancillas are omitted. The only class that cannot be excluded kinematically is the “cross” graph (c) with atom labels $\{1, \dots, 8\}$ and ports $\{1, 2, 3, 4\}$, see text.

(i) Assume there is at least one port connected to three or more ancillas. If this port is fixed as active, it blocks at least three ancillas. The resulting XNOR-complex on the three remaining ports has at most five atoms, which is impossible.

(ii) Assume at least one port connects to a single ancilla. Amputating this port yields a \bar{L}_{SCV} -complex with eight atoms. If an arbitrary port of this complex is fixed as active, the resulting complex has at most six atoms. Inspection of the language \bar{L}_{SCV} [Eq. (C1)] shows that this complex realizes the truth table of a XOR-gate, which, however, requires at least seven atoms (as shown in Appendix A 4).

(iii) Because of (i) and (ii), only the case that all ports connect to exactly two ancillas remains. There are six non-isomorphic bipartite graphs that connect sets of four (ports) and five vertices (ancillas), where all ports have degree 2, Fig. 13. We exclude graphs with disconnected ancillas because these are typically covered by the analogous step for $N = 8$. (Above we omitted this step to simplify the prove, so in principle here one has to check the graphs with disconnected ancillas too. The result is the same, though.) By inspection, one shows that all these graphs [except for the “cross” in Fig. 13(c)] allow for a pair of ports that when activated, block all ancillas of a third port (which then must be switched on as well). This, however, is inconsistent with the language L_{SCV} , which includes for all triples of ports states where two are on and one is off.

The “cross” graph in Fig. 13(c) cannot be excluded with this type of kinematic reasoning because the set of maximal independent sets [with the convention of ports shown in Fig. 13(c)] induces a superset of L_{SCV} . Therefore we have to use energetic arguments instead. With the atom indices shown in Fig. 13(c), the gap condition requires

$$\begin{aligned} E_{1111} &= -\Delta_1 - \Delta_2 - \Delta_3 - \Delta_4 \stackrel{!}{<} -\Delta_1 - \Delta_2 - \Delta_3 - \Delta_8 \\ &= E_{1110} \Rightarrow \Delta_8 < \Delta_4, \end{aligned} \quad (\text{C2a})$$

$$\begin{aligned} E_{1100} &= -\Delta_1 - \Delta_2 - \Delta_7 - \Delta_8 \stackrel{!}{<} -\Delta_1 - \Delta_2 - \Delta_7 - \Delta_4 \\ &= E_{1101} \Rightarrow \Delta_8 > \Delta_4. \end{aligned} \quad (\text{C2b})$$

Hence this graph cannot realize the L_{SCV} manifold.

(4) $N = 10$: To show that the surface code complex cannot be realized with $N = 10$ atoms, one follows the same procedure as detailed above for the case of $N = 9$ atoms (here we only briefly summarize the necessary steps): First, one excludes the case with ports that connect to a single ancilla (where one has to use that a $N = 9$ realization of a \bar{L}_{SCV} -complex can have only ports that connect to at least two ancillas). Then, one excludes the existence of ports that connect to at least four ancillas by using that XNOR-complexes cannot be realized with five atoms or less. Finally, one must exclude blockade graphs with ports of degree three or two by the same procedure as in Step (iii) above. In this case, there are 20 graph classes to cover of which 15 can be kinematically excluded and five can be energetically ruled out. These arguments show that the surface code vertex complex cannot be realized with 10 atoms. ■

2. Vertex complex for the Fibonacci model ($\mathcal{C}_{f_{\text{Fib}}}$)

Lemma 8. The vertex complex $\mathcal{C}_{f_{\text{Fib}}}$ of the Fibonacci model on the Honeycomb lattice cannot be realized with less than eight atoms.

Proof. The Fibonacci language $L_{\text{Fib}} = \{000, 011, 110, 101, 111\}$ contains the three states (011), (110), and (101), which we used in Appendix A 4 to show (with purely kinematic arguments) that XOR- and NAND-complexes cannot be realized with less than seven atoms. As the argument only relied on these three states (and the existence of at least one other state), it extends to the Fibonacci complex, which therefore also requires at least seven atoms. Furthermore, the three states forbid blockades between any two ports. So assume a realization with seven atoms exists. We distinguish three cases:

(1) At least one port connects to a single ancilla. Amputation (see the note in Appendix A 4) of this port yields a complex with six atoms that realizes the manifold $\bar{L}_{\text{Fib}} = \{100, 111, 010, 001, 011\}$ obtained from L_{Fib} by inverting the first letter (note that L_{Fib} is symmetric under permutations of ports). This language contains all XNOR states: $L_{\odot} \subset \bar{L}_{\text{Fib}}$. In Appendix A 5 we showed that there is only one blockade

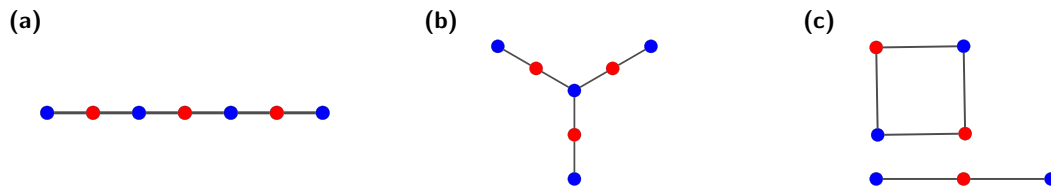


FIG. 14. The remaining three classes of blockade graphs for the Fibonacci vertex complex on seven atoms with ports of degree 2. Ports (ancillas) are colored red (blue) and connections between ancillas are omitted. Only the graph in (b) must be energetically excluded.

graph on 6 vertices that can realize these states; this graph has only four maximal independent sets and therefore cannot realize the additional state (011) in \bar{L}_{Fib} .

(2) At least one port connects to at least three ancillas. First, a port that connects to all *four* ancillas is inconsistent with two of the three states (011), (110), and (101). So assume there is a port that connects to *three* of the four ancillas. If this port is activated, it deactivates three ancillas and the remaining two ports (together with one ancilla) realize the irreducible language $L = \{01, 10, 11\}$ (the blockade graph of these three atoms must therefore be connected). But there is no graph on three vertices with (at least) three maximal independent sets of which (at least) one has (at least) two vertices.

(3) Because of (1) and (2), only the case where all ports connect to two ancillas remains. The possible classes of bipartite graphs are shown in Fig. 14. With a similar line of arguments as used for the surface code [Case (iii) for $N = 9$ in Appendix C 1], one can exclude two of the three graphs [(a) and (c)] with kinematic arguments [using the states (011), (110), and (101)]. The set of maximal independent sets for the

graph in Fig. 14(b) includes L_{Fib} as a subset and can again be excluded by energetic arguments. ■

APPENDIX D: NUMERICAL APPROACH FOR GEOMETRIC OPTIMIZATION

To minimize the objective function Γ on the high-dimensional configuration space \mathcal{C}_N , we used the SciPy method `scipy.optimize.dual_annealing` [85,97,98] that implements generalized simulated annealing [86,87] in combination with a local optimization based on the Nelder-Mead algorithm [88,89]. The stochastic algorithm starts from an initial geometry (which can be chosen randomly), followed by iterations of jumps in \mathcal{C}_N with probabilities that depend on the distance of the jump and the variation of the objective function Γ ; following each random jump, the Nelder-Mead algorithm optimizes the new configuration locally. After $\lesssim 2000$ iterations we stop the algorithm and compute the robustness of the final geometry. More technical details and all obtained optimal complexes can be found in Ref. [64]; the data of the optimized complexes can also be accessed online [90].

- [1] N. Schlosser, G. Reymond, I. Protsenko, and P. Grangier, Sub-poissonian loading of single atoms in a microscopic dipole trap, *Nature (London)* **411**, 1024 (2001).
- [2] M. Saffman, T. G. Walker, and K. Mølmer, Quantum information with Rydberg atoms, *Rev. Mod. Phys.* **82**, 2313 (2010).
- [3] F. Nogrette, H. Labuhn, S. Ravets, D. Barredo, L. Béguin, A. Vernier, T. Lahaye, and A. Browaeys, Single-Atom Trapping in Holographic 2D Arrays of Microtraps with Arbitrary Geometries, *Phys. Rev. X* **4**, 021034 (2014).
- [4] D. Barredo, S. de Léséleuc, V. Lienhard, T. Lahaye, and A. Browaeys, An atom-by-atom assembler of defect-free arbitrary two-dimensional atomic arrays, *Science* **354**, 1021 (2016).
- [5] D. Barredo, V. Lienhard, S. de Léséleuc, T. Lahaye, and A. Browaeys, Synthetic three-dimensional atomic structures assembled atom by atom, *Nature (London)* **561**, 79 (2018).
- [6] H. Weimer, M. Müller, I. Lesanovsky, P. Zoller, and H. P. Büchler, A Rydberg quantum simulator, *Nat. Phys.* **6**, 382 (2010).
- [7] I. Georgescu, S. Ashhab, and F. Nori, Quantum simulation, *Rev. Mod. Phys.* **86**, 153 (2014).
- [8] C. Gross, and I. Bloch, Quantum simulations with ultracold atoms in optical lattices, *Science* **357**, 995 (2017).
- [9] E. Altman, K. R. Brown, G. Carleo, L. D. Carr, E. Demler, C. Chin, B. DeMarco, S. E. Economou, M. A. Eriksson, Kai-Mei C. Fu, M. Greiner, K. R. A. Hazzard, R. G. Hulet, A. J. Kollar, B. L. Lev, M. D. Lukin, R. Ma, X. Mi, S. Misra, C. Monroe *et al.*, Quantum simulators: Architectures and opportunities, *PRX Quantum* **2**, 017003 (2021).
- [10] C. Degen, F. Reinhard, and P. Cappellaro, Quantum sensing, *Rev. Mod. Phys.* **89**, 035002 (2017).
- [11] L. Pezzè, A. Smerzi, M. K. Oberthaler, R. Schmied, and P. Treutlein, Quantum metrology with nonclassical states of atomic ensembles, *Rev. Mod. Phys.* **90**, 035005 (2018).
- [12] T. D. Ladd, F. Jelezko, R. Laflamme, Y. Nakamura, C. Monroe, and J. L. O'Brien, Quantum computers, *Nature (London)* **464**, 45 (2010).
- [13] L. Henriët, L. Béguin, A. Signoles, T. Lahaye, A. Browaeys, G.-O. Reymond, and C. Jurczak, Quantum computing with neutral atoms, *Quantum* **4**, 327 (2020).
- [14] T. M. Graham, Y. Song, J. Scott, C. Poole, L. Phuttitarn, K. Jooya, P. Eichler, X. Jiang, A. Marra, B. Grinkemeyer, M. Kwon, M. Ebert *et al.*, Multi-qubit entanglement and algorithms on a neutral-atom quantum computer, *Nature (London)* **604**, 457 (2022).
- [15] D. Bluvstein, H. Levine, G. Semeghini, T. T. Wang, S. Ebadi, M. Kalinowski, A. Keesling, N. Maskara, H. Pichler, M. Greiner *et al.*, A quantum processor based on coherent transport of entangled atom arrays, *Nature (London)* **604**, 451 (2022).
- [16] T. Gallagher, Rydberg atoms, in *Springer Handbook of Atomic, Molecular, and Optical Physics* (Springer, New York, 2006), pp. 235–245.

- [17] N. Sibalic and C. S. Adams, *Rydberg Physics* (IOP Publishing, Bristol, 2018).
- [18] D. Jaksch, J. I. Cirac, P. Zoller, S. L. Rolston, R. Côté, and M. D. Lukin, Fast Quantum Gates for Neutral Atoms, *Phys. Rev. Lett.* **85**, 2208 (2000).
- [19] D. Tong, S. M. Farooqi, J. Stanojevic, S. Krishnan, Y. P. Zhang, R. Côté, E. E. Eyler, and P. L. Gould, Local Blockade of Rydberg Excitation in an Ultracold Gas, *Phys. Rev. Lett.* **93**, 063001 (2004).
- [20] K. Singer, M. Reetz-Lamour, T. Amthor, L. G. Marcassa, and M. Weidemüller, Suppression of Excitation and Spectral Broadening Induced by Interactions in a Cold Gas of Rydberg Atoms, *Phys. Rev. Lett.* **93**, 163001 (2004).
- [21] A. Gaëtan, Y. Miroshnychenko, T. Wilk, A. Chotia, M. Viteau, D. Comparat, P. Pilllet, A. Browaeys, and P. Grangier, Observation of collective excitation of two individual atoms in the Rydberg blockade regime, *Nat. Phys.* **5**, 115 (2009).
- [22] E. Urban, T. A. Johnson, T. Henage, L. Isenhower, D. D. Yavuz, T. G. Walker, and M. Saffman, Observation of Rydberg blockade between two atoms, *Nat. Phys.* **5**, 110 (2009).
- [23] S. Ebadi, T. T. Wang, H. Levine, A. Keesling, G. Semeghini, A. Omran, D. Bluvstein, R. Samajdar, H. Pichler, W. W. Ho, S. Choi, S. Sachdev *et al.*, Quantum phases of matter on a 256-atom programmable quantum simulator, *Nature (London)* **595**, 227 (2021).
- [24] P. Scholl, M. Schuler, H. J. Williams, A. A. Eberharter, D. Barredo, K.-N. Schymik, V. Lienhard, L.-P. Henry, T. C. Lang, T. Lahaye *et al.*, Quantum simulation of 2D antiferromagnets with hundreds of Rydberg atoms, *Nature (London)* **595**, 233 (2021).
- [25] K.-N. Schymik, B. Ximenez, E. Bloch, D. Dreon, A. Signoles, F. Nogrette, D. Barredo, A. Browaeys, and T. Lahaye, *In situ* equalization of single-atom loading in large-scale optical tweezer arrays, *Phys. Rev. A* **106**, 022611 (2022).
- [26] NISQ = Noisy intermediate-scale quantum technology, i.e., near-term quantum technology without full-fledged quantum error correction, see Ref. [95].
- [27] H. Pichler, S.-T. Wang, L. Zhou, S. Choi, and M. D. Lukin, Quantum optimization for maximum independent set using Rydberg atom arrays, [arXiv:1808.10816](https://arxiv.org/abs/1808.10816).
- [28] B. N. Clark, C. J. Colbourn, and D. S. Johnson, Unit disk graphs, *Discrete Math.* **86**, 165 (1990).
- [29] H. Pichler, S.-T. Wang, L. Zhou, S. Choi, and M. D. Lukin, Computational complexity of the Rydberg blockade in two dimensions, [arXiv:1809.04954](https://arxiv.org/abs/1809.04954).
- [30] M. F. Serret, B. Marchand, and T. Ayril, Solving optimization problems with Rydberg analog quantum computers: Realistic requirements for quantum advantage using noisy simulation and classical benchmarks, *Phys. Rev. A* **102**, 052617 (2020).
- [31] J. Wurtz, P. L. S. Lopes, N. Gemelke, A. Keesling, and S. Wang, Industry applications of neutral-atom quantum computing solving independent set problems, [arXiv:2205.08500](https://arxiv.org/abs/2205.08500).
- [32] C. Dalyac and L. Henriët, Embedding the MIS problem for non-local graphs with bounded degree using 3D arrays of atoms, [arXiv:2209.05164](https://arxiv.org/abs/2209.05164).
- [33] M.-T. Nguyen, J.-G. Liu, J. Wurtz, M. D. Lukin, S.-T. Wang, and H. Pichler, Quantum optimization with arbitrary connectivity using Rydberg atom arrays, *PRX Quantum* **4**, 010316 (2023).
- [34] M. Lanthaler, C. Daska, K. Ender, and W. Lechner, Rydberg-Blockade-Based Parity Quantum Optimization, *Phys. Rev. Lett.* **130**, 220601 (2023).
- [35] S. Jeong, M. Kim, M. Hhan, and J. Ahn, Quantum programming of the satisfiability problem with Rydberg atom graphs, [arXiv:2302.14369](https://arxiv.org/abs/2302.14369).
- [36] Of course one should not expect an exponential speedup by these mappings as it is widely believed [96] that $NP \not\subseteq BQP$.
- [37] A. Byun, M. Kim, and J. Ahn, Finding the maximum independent sets of platonic graphs using Rydberg atoms, *PRX Quantum* **3**, 030305 (2022).
- [38] M. Kim, K. Kim, J. Hwang, E.-G. Moon, and J. Ahn, Rydberg quantum wires for maximum independent set problems, *Nat. Phys.* **18**, 755 (2022).
- [39] S. Ebadi, A. Keesling, M. Cain, T. T. Wang, H. Levine, D. Bluvstein, G. Semeghini, A. Omran, J.-G. Liu, R. Samajdar *et al.*, Quantum optimization of maximum independent set using Rydberg atom arrays, *Science* **376**, 1209 (2022).
- [40] A. Celi, B. Vermersch, O. Viyuela, H. Pichler, M. D. Lukin, and P. Zoller, Emerging Two-Dimensional Gauge Theories in Rydberg Configurable Arrays, *Phys. Rev. X* **10**, 021057 (2020).
- [41] R. Verresen, M. D. Lukin, and A. Vishwanath, Prediction of Toric Code Topological Order from Rydberg Blockade, *Phys. Rev. X* **11**, 031005 (2021).
- [42] R. Samajdar, W. W. Ho, H. Pichler, M. D. Lukin, and S. Sachdev, Quantum phases of Rydberg atoms on a kagome lattice, *Proc. Natl. Acad. Sci. USA* **118**, e2015785118 (2021).
- [43] R. Moessner, S. L. Sondhi, and E. Fradkin, Short-ranged resonating valence bond physics, quantum dimer models, and Ising gauge theories, *Phys. Rev. B* **65**, 024504 (2001).
- [44] G. Semeghini, H. Levine, A. Keesling, S. Ebadi, T. T. Wang, D. Bluvstein, R. Verresen, H. Pichler, M. Kalinowski, R. Samajdar, A. Omran, S. Sachdev *et al.*, Probing topological spin liquids on a programmable quantum simulator, *Science* **374**, 1242 (2021).
- [45] G. Giudici, M. D. Lukin, and H. Pichler, Dynamical Preparation of Quantum Spin Liquids in Rydberg Atom Arrays, *Phys. Rev. Lett.* **129**, 090401 (2022).
- [46] R. Sahay, A. Vishwanath, and R. Verresen, Quantum spin puddles and lakes: NISQ-era spin liquids from non-equilibrium dynamics, [arXiv:2211.01381](https://arxiv.org/abs/2211.01381).
- [47] A. Kitaev, Fault-tolerant quantum computation by anyons, *Ann. Phys.* **303**, 2 (2003).
- [48] M. A. Levin and X.-G. Wen, String-net condensation: A physical mechanism for topological phases, *Phys. Rev. B* **71**, 045110 (2005).
- [49] To prevent misconceptions, we stress that the term “complex” in “Rydberg complex” refers to a *spatial arrangement* of Rydberg atoms (with additional data) and is *not* related to the mathematical concept of an *independence complex*, i.e., the family of independent sets of a graph.
- [50] M. D. Lukin, M. Fleischhauer, R. Cote, L. M. Duan, D. Jaksch, J. I. Cirac, and P. Zoller, Dipole Blockade and Quantum Information Processing in Mesoscopic Atomic Ensembles, *Phys. Rev. Lett.* **87**, 037901 (2001).
- [51] P. Schauf, J. Zeiher, T. Fukuhara, S. Hild, M. Cheneau, T. Macrì, T. Pohl, I. Bloch, and C. Gross, Crystallization in Ising quantum magnets, *Science* **347**, 1455 (2015).
- [52] H. Labuhn, D. Barredo, S. Ravets, S. de Léséleuc, T. Macrì, T. Lahaye, and A. Browaeys, Tunable two-dimensional arrays

- of single Rydberg atoms for realizing quantum Ising models, *Nature (London)* **534**, 667 (2016).
- [53] H. Bernien, S. Schwartz, A. Keesling, H. Levine, A. Omran, H. Pichler, S. Choi, A. S. Zibrov, M. Endres, M. Greiner *et al.*, Probing many-body dynamics on a 51-atom quantum simulator, *Nature (London)* **551**, 579 (2017).
- [54] H. Labuhn, S. Ravets, D. Barredo, L. Béguin, F. Nogrette, T. Lahaye, and A. Browaeys, Single-atom addressing in microtraps for quantum-state engineering using Rydberg atoms, *Phys. Rev. A* **90**, 023415 (2014).
- [55] A. Omran, H. Levine, A. Keesling, G. Semeghini, T. T. Wang, S. Ebadi, H. Bernien, A. S. Zibrov, H. Pichler, S. Choi *et al.*, Generation and manipulation of Schrödinger cat states in Rydberg atom arrays, *Science* **365**, 570 (2019).
- [56] I. Lesanovsky, Many-Body Spin Interactions and the Ground State of a Dense Rydberg Lattice Gas, *Phys. Rev. Lett.* **106**, 025301 (2011).
- [57] A. Browaeys, and T. Lahaye, Many-body physics with individually controlled Rydberg atoms, *Nat. Phys.* **16**, 132 (2020).
- [58] M. Davis, R. Sigal, and E. Weyuker, *Computability, Complexity, and Languages: Fundamentals of Theoretical Computer Science, Computer Science and Scientific Computing* (Elsevier Science, Amsterdam, 1994).
- [59] J. B. Kogut, An introduction to lattice gauge theory and spin systems, *Rev. Mod. Phys.* **51**, 659 (1979).
- [60] Here, *disjoint* means that $(x, y) \neq (x', y')$ implies $x \neq x'$ and $y \neq y'$; thus γ can be interpreted as a *partial bijection* between character positions of the two languages L_1 and L_2 .
- [61] W. Wernick, Complete sets of logical functions, *Trans. Am. Math. Soc.* **51**, 117 (1942).
- [62] H. M. Sheffer, A set of five independent postulates for Boolean algebras, with application to logical constants, *Trans. Am. Math. Soc.* **14**, 481 (1913).
- [63] A. K. Dewdney, Logic circuits in the plane, *ACM SIGACT News* **10**, 38 (1979).
- [64] S. Stastny, Functional Rydberg complexes in the PXP-Model, Master's thesis, University of Stuttgart, Stuttgart, 2023.
- [65] S. B. Bravyi and A. Y. Kitaev, Quantum codes on a lattice with boundary, [arXiv:quant-ph/9811052](https://arxiv.org/abs/quant-ph/9811052).
- [66] A. Kitaev, Anyons in an exactly solved model and beyond, *Ann. Phys.* **321**, 2 (2006).
- [67] E. Dennis, A. Kitaev, A. Landahl, and J. Preskill, Topological quantum memory, *J. Math. Phys.* **43**, 4452 (2002).
- [68] R. Barends, J. Kelly, A. Megrant, A. Veitia, D. Sank, E. Jeffrey, T. C. White, J. Mutus, A. G. Fowler, B. Campbell *et al.*, Superconducting quantum circuits at the surface code threshold for fault tolerance, *Nature (London)* **508**, 500 (2014).
- [69] J. Kelly, R. Barends, A. G. Fowler, A. Megrant, E. Jeffrey, T. C. White, D. Sank, J. Y. Mutus, B. Campbell, Y. Chen *et al.*, State preservation by repetitive error detection in a superconducting quantum circuit, *Nature (London)* **519**, 66 (2015).
- [70] A. Kitaev and J. Preskill, Topological Entanglement Entropy, *Phys. Rev. Lett.* **96**, 110404 (2006).
- [71] M. Levin and X.-G. Wen, Detecting Topological Order in a Ground State Wave Function, *Phys. Rev. Lett.* **96**, 110405 (2006).
- [72] M. H. Freedman, A. Kitaev, M. J. Larsen, and Z. Wang, Topological quantum computation, *Bull. Am. Math. Soc.* **40**, 31 (2003).
- [73] C. Nayak, S. H. Simon, A. Stern, M. Freedman, and S. Das Sarma, Non-Abelian anyons and topological quantum computation, *Rev. Mod. Phys.* **80**, 1083 (2008).
- [74] Z. Wang, *Topological Quantum Computation*, No. 112 in Regional Conference Series in Mathematics/Conference Board of the Mathematical Sciences (American Mathematical Society, Providence, Rhode Island, 2010).
- [75] M. H. Freedman, M. Larsen, and Z. Wang, A modular functor which is universal for quantum computation, *Commun. Math. Phys.* **227**, 605 (2002).
- [76] J. Preskill, *Lecture Notes for Physics 219: Quantumcomputation* (2004), available at <http://theory.caltech.edu/preskill/ph219/topological.pdf>.
- [77] N. E. Bonesteel, L. Hormozi, G. Zikos, and S. H. Simon, Braid Topologies for Quantum Computation, *Phys. Rev. Lett.* **95**, 140503 (2005).
- [78] N. Read and E. Rezayi, Beyond paired quantum Hall states: Parafermions and incompressible states in the first excited Landau level, *Phys. Rev. B* **59**, 8084 (1999).
- [79] J. S. Xia, W. Pan, C. L. Vicente, E. D. Adams, N. S. Sullivan, H. L. Stormer, D. C. Tsui, L. N. Pfeiffer, K. W. Baldwin, and K. W. West, Electron Correlation in the Second Landau Level: A Competition Between Many Nearly Degenerate Quantum Phases, *Phys. Rev. Lett.* **93**, 176809 (2004).
- [80] L. Fidkowski, M. Freedman, C. Nayak, K. Walker, and Z. Wang, From string nets to nonabelions, *Commun. Math. Phys.* **287**, 805 (2009).
- [81] P. Fendley, Topological order from quantum loops and nets, *Ann. Phys.* **323**, 3113 (2008).
- [82] S. H. Simon and P. Fendley, Exactly solvable lattice models with crossing symmetry, *J. Phys. A: Math. Theor.* **46**, 105002 (2013).
- [83] M. D. Schulz, S. Dusuel, K. P. Schmidt, and J. Vidal, Topological Phase Transitions in the Golden String-Net Model, *Phys. Rev. Lett.* **110**, 147203 (2013).
- [84] H. Breu and D. G. Kirkpatrick, Unit disk graph recognition is NP-hard, *Comput. Geometry* **9**, 3 (1998).
- [85] P. Virtanen, R. Gommers, T. E. Oliphant, M. Haberland, T. Reddy, D. Cournapeau, E. Burovski, P. Peterson, W. Weckesser, J. Bright *et al.*, SciPy 1.0: fundamental algorithms for scientific computing in python, *Nat. Methods* **17**, 261 (2020).
- [86] C. Tsallis and D. A. Stariolo, Generalized simulated annealing, *Physica A: Statis. Mech. Appl.* **233**, 395 (1996).
- [87] I. Andricioaei and J. E. Straub, Generalized simulated annealing algorithms using Tsallis statistics: Application to conformational optimization of a tetrapeptide, *Phys. Rev. E* **53**, R3055 (1996).
- [88] J. A. Nelder and R. Mead, A simplex method for function minimization, *Comput. J.* **7**, 308 (1965).
- [89] F. Gao and L. Han, Implementing the Nelder-Mead simplex algorithm with adaptive parameters, *Comput. Optim. Appl.* **51**, 259 (2012).
- [90] S. Stastny, H. P. Büchler, and N. Lang, *Data for "Functional Completeness of Planar Rydberg Blockade Structures"*, <https://doi.org/10.18419/darus-3307>.
- [91] J. Gross, J. Yellen, and P. Zhang, *Handbook of Graph Theory*, 2nd ed., Discrete Mathematics and Its Applications (Taylor & Francis, London, 2013).

- [92] C. McDiarmid and T. Müller, Integer realizations of disk and segment graphs, *J. Comb. Theory, Ser. B* **103**, 114 (2013).
- [93] F. Kuhn, T. Moscibroda, and R. Wattenhofer, Unit disk graph approximation, in *Proceedings of the 2004 Joint Workshop on Foundations of Mobile Computing: DIALM-POMC '04* (ACM Press, New York, NY, 2004).
- [94] S. Bravyi, D. P. DiVincenzo, and D. Loss, Schrieffer-Wolff transformation for quantum many-body systems, *Ann. Phys.* **326**, 2793 (2011).
- [95] J. Preskill, Quantum computing in the NISQ era and beyond, *Quantum* **2**, 79 (2018).
- [96] C. H. Bennett, E. Bernstein, G. Brassard and U. Vazirani, Strengths and weaknesses of quantum computing, *SIAM J. Comput.* **26**, 1510 (1997).
- [97] Y. Xiang, D. Sun, W. Fan, and X. Gong, Generalized simulated annealing algorithm and its application to the Thomson model, *Phys. Lett. A* **233**, 216 (1997).
- [98] Y. Xiang and X. G. Gong, Efficiency of generalized simulated annealing, *Phys. Rev. E* **62**, 4473 (2000).